NEUTRON CAPTURE CROSS SECTIONS

IN THE KEV REGION

by

EDWARD GEORGE BILPUCH

A thesis submitted to the Faculty of
the University of North Carolina in
partial fulfillment of the requirements
for the degree of Doctor of Philosophy
in the Department of Physics

Henry W Newson

Chapel Hill

1956

Approved by:

_____

Adviser

ACKNOWLEDGEMENTS

The author wishes to express his appreciation and gratitude to Professor N. D. Palmatier, of the University of North Carolina, and to Professor H. W. Newson, of Duke University, for their guidance and helpful discussions throughout the course of this experiment.

My thanks are also extended to Dr. R. H. Rohrer, now at Emory University, whose assistance in the preliminary phases of this work was very valuable. Thanks are also extended to the Van de Graaff group at Duke University for their assistance in taking data.

This work was supported by the Atomic Energy Commission.

TABLE OF CONTENTS

LIST OF FIGURES

CHAPTER I

INTRODUCTION

The strong fluctuations which nuclear cross sections exhibit are called resonances. From these resonances, we can obtain the spacings of the nuclear energy levels and their natural widths for levels approximately 8 Mev above the ground state. These observable quantities play an important role in the determination of a satisfactory nuclear model.

Neutrons with a well defined energy are needed to investigate the cross section resonances. For neutron energies ranging from .02 ev to 20 ev, crystal diffraction instruments are used (W4)*; and for energies ranging from 2 ev to 500 ev, time-of-flight methods are used (S2). The resonance region has been the focus of attention in many laboratories, and the resonances have been analyzed for many of the elements. The quantities obtained from analyzing an individual resonance are the width of the level, the neutron width and radiation width. These quantities are called the resonance parameters and are obtained from total cross section measurements.

For neutron energies above 50 kev, the average neutron capture cross sections have been measured at Los Alamos (A1) for many elements. Very little work has been done in the lower kev region. Therefore, the main purpose of this present work is to investigate the region from 3 kev

---

*References will be denoted in brackets ( ). These are then given in the bibliography.

to 250 kev by finding the average capture cross sections. Because individual levels of heavy elements cannot be resolved with neutrons produced by the Van de Graaff, we can only measure the average capture cross sections. Once the cross sections are known for the region, we will be able to compare the Los Alamos absolute cross sections to the Brookhaven resonance parameters. We will, in effect, bridge the gap between the resonance region and the region above 50 kev.

In order to achieve the above stated purpose, we need only obtain relative cross section curves. This work was purposely designed to overlap the Los Alamos region in order to match the shapes of the cross section curves. If the curves match, then we can normalize our cross sections to the absolute cross sections given by Los Alamos. We then obtain an absolute cross section down to 3 kev. By using the current theory for nuclear cross sections and the experimental resonance parameters, we can calculate the capture cross section for the region 3 kev to 250 kev.

Our original intention was to make an absolute calibration independent of the Los Alamos points. This was not done because a calibrated neutron source was not available at the completion of this work. Plans have been made to obtain a calibrated source, and the absolute measurement of the cross sections will be made in the near future.

In the kev region, there are two ways in which we can measure the capture cross section directly. First, we can measure the gamma radiation given off by a nucleus immediately after it has captured a

neutron. Second, many nuclei become radioactive after neutron capture, and we can measure the amount of induced activity which is related to the capture process. The former method is not applicable in the present work because of the high gamma radiation associated with the electrostatic generator. Besides, we use the $Li^{7}(p,n)Be^{7}$ reaction as our source of neutrons, and this reaction also produces many gamma rays.

By studying the induced activity, we are restricted to those nuclei which can be activated and which have a convenient half-life for decay. On the other hand, the great advantage of this method is that we do not always need separated isotopes; the half-lives enable us to assign the induced activities to the proper isotopes. Another advantage of activation experiments is that we can use oxides as samples. This is due to the fact that O^{16} (99.76% abundant) and O^{17} are stable upon neutron capture. These isotopes would have to undergo several successive neutron captures to O^{19} in order to show any beta activity. O^{18}, which is 0.2% abundant, becomes beta active when it captures a neutron, and the half-life is 29 seconds. Since only a very small amount of O^{18} is present in a sample and since the half-life of O^{19} is short, we can conclude thatthe beta activity will not be observed.

Neutron capture cross sections are also important in the study of the abundance of elements in the universe (G1). Recently, Fowler and Burbidge (F3, F4) have published several articles on the origin of the elements and their abundances. This current theory predicts that element-building reactions are continually taking place in stars. After the lighter elements are produced, the heavy elements are synthesized by

successive neutron capture and beta decay processes. The temperature at the core of stars corresponds to $kT \approx 10$ kev. Therefore, neutron capture cross sections near this energy are very important in the build-up process.

If one were to study a chart of the isotopes, he would see that the elements can be synthesized in such a manner. Therefore, neutron capture cross sections near 10 kev are of fundamental importance if we are to understand better the Universe in which we live.

CHAPTER II

THEORY FOR NEUTRON CAPTURE CROSS SECTIONS

In 1936, Breit and Wigner (B4) developed a theory for nuclear resonances and obtained an expression that was analogous to that used in the theory of optical dispersion. Later workers (F1, W1, W2), using the partial wave picture, developed the Breit-Wigner equations into a form more useful for experiments today. The equations, in the neighborhood of a single resonance, may be written (B3, Pages 393-4):

Capture Cross Section, $$\sigma_\gamma = (2l+1)g' \pi \lambda\!\!\!^{-2} \frac{\Gamma_n \Gamma_\gamma}{(E-E_0)^2 + \Gamma^2/4} \qquad 2.1$$

Scattering Cross Section,

$$\sigma_s = (2l+1)\, g' \pi \lambda\!\!\!^{-2} \left| \frac{i\,\Gamma_n}{E - E_0 + i\,\Gamma/2} + A^l_{pot.} \right|^2 \qquad 2.2$$

In this work, we will only be concerned with the capture cross section. In the expression 2.1, l is the angular momentum of the incident neutron; $2\pi\lambda\!\!\!^{-}$ is the de Broglie wavelength associated with the neutron; Γ_n is the neutron width; Γ_γ is the radiation width and $\Gamma = \Gamma_n + \Gamma_\gamma$ is the total width of the level in the compound nucleus. E is the energy of the incident neutron and E_0 is the neutron energy at the resonance; g' is a function of the spin, I, of the target nucleus, and the total spin of the compound nucleus, J. It is given by:

$$(2l+1)g' = \frac{1}{2}\left(\frac{2J+1}{2I+1}\right) \qquad 2.3$$

In 1947, Feshbach, Peaslee and Weisskopf (F1) proposed a nuclear

model which predicted that the ratio $\overline{\Gamma n^0}/\overline{D}$ for neutrons was constant, i.e. independent of atomic weight. $\overline{\Gamma n^0}$ is the average reduced neutron width over many levels where $\Gamma n^0 = \Gamma n / \sqrt{E_0}\, v_\ell$ and $\overline{D}$ is the average level spacing. v_ℓ is the barrier penetration factor and is dependent on the angular momentum of the incident neutron. It will be discussed in greater detail in a later section. Here we need only say that for $\ell = 0$ neutrons $v_0 = 1$. This model, commonly referred to as the black-nucleus model, is a very poor approximation.

Later total cross section experiments showed that the ratio, $\overline{\Gamma n^0}/\overline{D}$, had maxima for s-wave neutrons in the neighborhood of atomic weights 11, 55, 155.

In 1953, Feshbach, Porter and Weisskopf (F2) proposed a theory which predicted a variation of the $\overline{\Gamma n^0}/\overline{D}$ ratio with atomic weight. This model is commonly referred to as the cloudy crystal-ball model and assumes a complex nuclear potential well. For a well depth of about 42 Mev, this model predicts maxima in $\overline{\Gamma n^0}/\overline{D}$ for s-wave neutrons at atomic weights of 11, 55 and 155.

Carter, et al (C2) have plotted the experimental ratios in the neighborhood of atomic weight 155. These experimental ratios for s-wave neutrons peak at about mass 160, and this peak is somewhat lower than the expected peak. Hence, the experimental values indicate a well depth somewhat less than 42 Mev.

THE RESONANCE INTEGRAL AND THE AVERAGE σ_a FOR ℓ=0 NEUTRONS

In the kev region, it is known that the levels are closely

spaced for most heavy nuclei and that each energy interval of a few kev contains many resonance levels. We will first calculate the resonant integral for a single level:

$$\Sigma_a = \int_{E_0-D_1}^{E_0+D_2} \frac{\sigma_a(E)\,dE}{D_1+D_2} \qquad 2.4$$

We assume that the neutrons have a uniform distribution over the interval $D_1 + D_2$ where $D = D_1 + D_2$. σ_n (as given by equation 2.1) and Σ_a are in the same units.

The resonant integral is the average capture cross section over the resonance. Since one resonance is contained within each interval D, we can write for s-wave neutrons:

$$\Sigma_a = \frac{g'\pi\lambda^2}{D} \int_{E_0-D_1}^{E_0+D_2} \frac{\Gamma_n\Gamma_\gamma}{(E-E_0)^2+\left(\frac{\Gamma}{2}\right)^2}\,dE \qquad 2.5$$

Γ_γ is constant and Γ_n is a slowly varying function of energy which can be considered constant over the interval D. Also, since only the immediate neighborhood of the resonance contributes to the integral, we can extend the limits from $-\infty$ to $+\infty$. Therefore, we have:

$$\Sigma_a = \frac{g'\pi\lambda^2\Gamma_n\Gamma_\gamma}{D} \int_{-\infty}^{\infty} \frac{dE}{(E-E_0)^2+(\Gamma/2)^2} \qquad 2.6$$

Performing the integration and evaluating the constants, we obtain the average cross section over the interval D. This expression, given in barns, is:

$$\Sigma_a = g'\frac{\pi}{2}\left(\frac{2.6\times10^4}{E_0}\right)\frac{\Gamma_\gamma}{D}\,\frac{\Gamma_n}{\Gamma_n+\Gamma_\gamma} \qquad 2.7$$

where E_o is in electron volts. $\Gamma_n = \Gamma_n^o \sqrt{E_o}$ where Γ_n^o is the neutron reduced width.

The parameters Γ_γ, D and Γ_n^o differ from level to level. If $\sigma_a(E)$ is measured with a neutron energy spread $\Delta E \leq D$, very considerable fluctuations will be observed. When $\Delta E \gg D$, a smooth average capture cross section (as a function of energy) is observed which depends on the value of these parameters averaged over many levels. However, if a uniform distribution is assumed, i.e. that Γ_n^o is approximately the same for all ($\ell = 0$) levels in an energy interval ΔE and that Γ_γ is approximately the same for all ($\ell = 0$) levels in the same interval, then

$$(\sigma_a)_{\substack{Ave \\ \ell=0}} = g' \frac{\pi}{2} \left(\frac{2.6 \times 10^6}{E_m}\right) \frac{\bar{\Gamma}_\gamma}{D} \frac{\bar{\Gamma}_n}{\bar{\Gamma}_n + \bar{\Gamma}_\gamma} \qquad 2.7a$$

where E_m is the average neutron energy in the interval ΔE. This expression is a poor approximation except where $\bar{\Gamma}_n \gg \bar{\Gamma}_\gamma$ or $\bar{\Gamma}_n \ll \bar{\Gamma}_\gamma$.

THE AVERAGE $\sigma_a(E)$ FOR DISTRIBUTION FUNCTION e^{-y} AND $\ell = 0$

In the program of work carried out by the Brookhaven group (H11), it was discovered that Γ_γ was nearly the same but the reduced neutron width, Γ_n^o, had an extremely large variation in size from level to level of a given nuclide. Hughes and Harvey (H11) then proposed a distribution function for the reduced neutron width. The distribution function is e^{-y} where $y = \Gamma_n^o / \bar{\Gamma}_n^o$ and seems to fit the experimental data rather well.

Equation 2.7a can be written:

$$(\sigma_a)_{\substack{Ave \\ \ell=0}} = g' \frac{\pi}{2} \left(\frac{2.6 \times 10^6}{E_m}\right) \frac{\Gamma_n^o}{\Gamma_n^o + b} \frac{\bar{\Gamma}_\gamma}{D} \qquad 2.7b$$

where $b = \frac{\Gamma_\gamma}{\sqrt{E_n}}$

We now introduce the normalized distribution function into the above expression and integrate from 0 to ∞. This will give a better approximation to the average cross section and will be designated by $(\bar{\sigma}_n)$.

$$(\bar{\sigma}_a)_{\ell=0} = g' \frac{\pi}{2}\left(\frac{2.6\times10^6}{E_n}\right)\frac{\Gamma_\gamma}{\bar{D}\bar{\Gamma}_n^0}\int_0^\infty e^{-\Gamma_n^0/\bar{\Gamma}_n^0}\frac{\Gamma_n^0}{\Gamma_n^0+b}\,d\Gamma_n^0 \qquad 2.8$$

Integrating this expression, we obtain for s-wave neutrons:

$$(\bar{\sigma}_a)_{\ell=0} = g' \frac{\pi}{2}\left(\frac{2.6\times10^6}{E_n}\right)\frac{\Gamma_\gamma}{\bar{D}}\left[1 - x_0 e^{x_0}\int_{x_0}^\infty \frac{e^{-x}}{x}\,dx\right] \qquad 2.9$$

where $X_0 = \frac{\Gamma_\gamma}{\bar{\Gamma}_n^0\sqrt{E_n}}$

The definite integral in 2.9 is a tabulated function (T1) for values of X_0 up to 15. For values of $X_0 > 15$. the integral can be expanded into an infinite series.

$$(\bar{\sigma}_a)_{\ell=0} = g' \frac{\pi}{2}\left(\frac{2.6\times10^6}{E_n}\right)\frac{\Gamma_\gamma}{\bar{D}}\left[\frac{1!}{X_0} - \frac{2!}{X_0^2} + \frac{3!}{X_0^3} + \text{-----}\right] \qquad 2.10$$

Therefore, for large X_0 ($X_0 > 15$), we need only the first few terms of the series in order to obtain $(\bar{\Gamma}_n)$.

THE AVERAGE σ_a (E) FOR DISTRIBUTION FUNCTION $e^{-y^2/4}/(y)^{\frac{1}{2}}$ AND $\ell = 0$

Porter and Thomas (T3) analyzed the existing data and proposed the distribution $e^{-y^2/4}/(y)^{\frac{1}{2}}$ as one more likely to be correct than the distribution e^{-y}. The Porter-Thomas distribution also has some theoretical justification.

By substituting this distribution into equation 2.7b and

integrating from 0 to ∞ we obtain:

$$(\bar{\sigma}_a)_{\ell=0} = g' \frac{\pi}{2}\left(\frac{2.6\times10^6}{E_n}\right)\frac{\Gamma_\gamma}{D}\frac{1}{\sqrt{2\pi}\,\bar{\Gamma}_n^0}\left[\frac{1}{\sqrt{2}}\int_0^\infty \frac{e^{-\Gamma_n^0/2\bar{\Gamma}_n^0}}{\left(\frac{\Gamma_n^0}{2\bar{\Gamma}_n^0}\right)^{1/2}}\frac{\Gamma_n^0\, d\Gamma_n^0}{\Gamma_n^0+\frac{\Gamma_\gamma}{\sqrt{E_n}}}\right] \qquad 2.11$$

where $\frac{1}{\sqrt{2\pi}\,\bar{\Gamma}_n^0}$ is the normalizing factor for the distribution. If we divide the numerator and denominator of the integral by $2\bar{\Gamma}_n^0$ and make the substitutions $v^2 = \frac{\Gamma_n^0}{2\bar{\Gamma}_n^0}$ and $b = \frac{\Gamma_\gamma}{2\bar{\Gamma}_n^0\sqrt{E_n}}$ we obtain:

$$(\bar{\sigma}_a)_{\ell=0} = g'\pi\left(\frac{2.6\times10^6}{E_n}\right)\frac{\Gamma_\gamma}{D\sqrt{\pi}}\int_0^\infty \frac{v^2 e^{-v^2}}{v^2+b}\,dv \qquad 2.12$$

The solution of the integral in equation 2.12 is given in the appendix. Here we will only use the end result.

$$(\bar{\sigma}_a)_{\ell=0} = g'\frac{\pi}{2}\left(\frac{2.6\times10^6}{E_n}\right)\frac{\Gamma_\gamma}{D}\left[1-\sqrt{b\pi}\,e^b\left(1-\frac{2}{\sqrt{\pi}}\int_0^{\sqrt{b}} e^{-t^2}dt\right)\right] \qquad 2.13$$

where $b = \frac{\Gamma_\gamma}{2\bar{\Gamma}_n^0\sqrt{E_n}}$

The above integral is the error function and is tabulated (T2).

The expressions 2.7, 2.9, 2.10 and 2.13 give the average capture cross section for s-wave neutrons on the basis of different distribution functions. The way in which the distributions effect the average capture cross section for U^{238} is shown in Fig. 1. For each distribution, the same parameters were used. They are: $\bar{D}$ = 19 ev, Γ_γ = 23 mv and $\bar{\Gamma}_n^0$ = 2.8 mv.

The expressions derived in this section and the following section are valid only when $E_0 \pm E_n \gg \bar{D}$. They are also valid only for thin samples where we can assume that the neutron flux is constant throughout

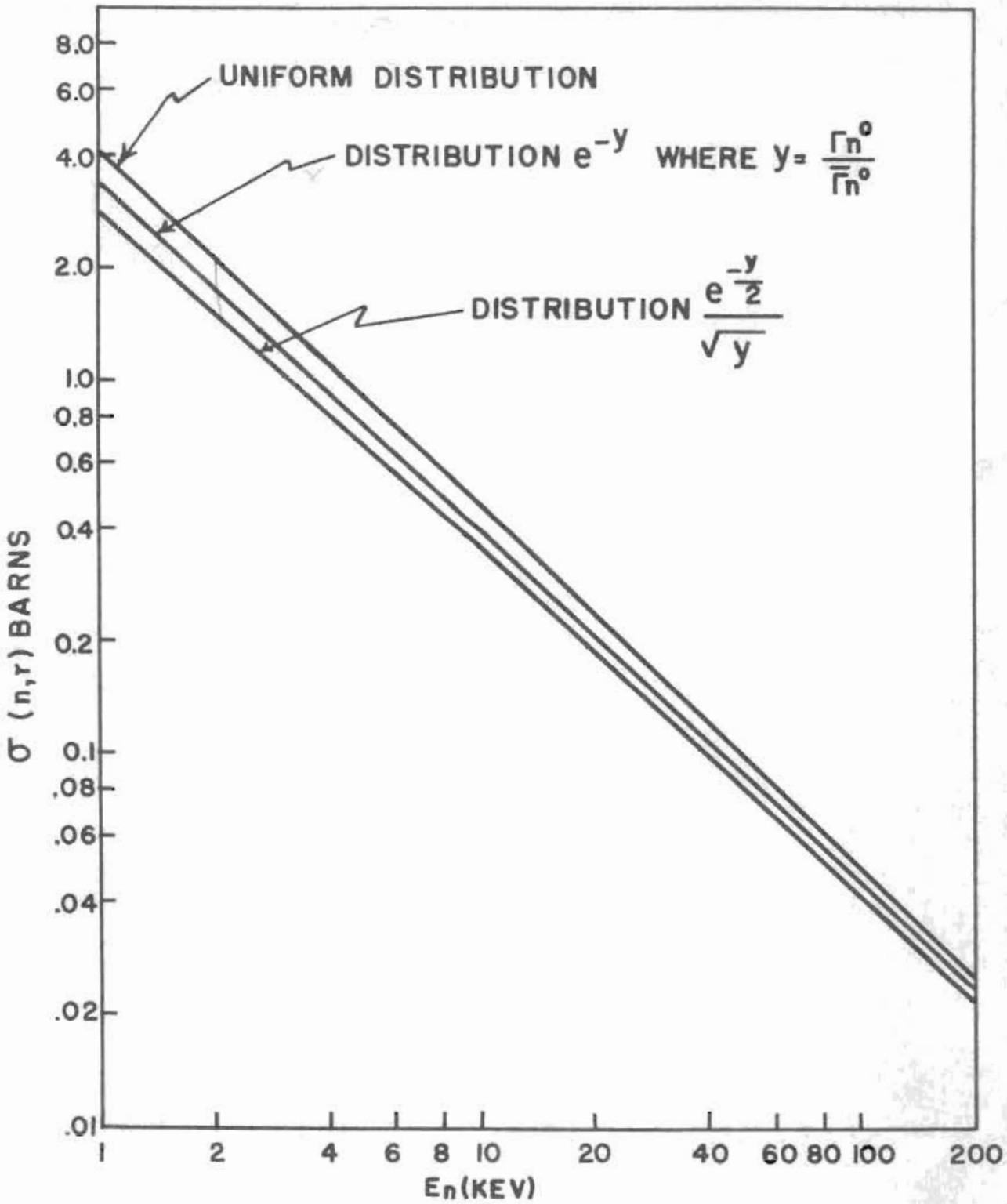

FIG I S-WAVE CONTRIBUTION TO CAPTURE CROSS SECTION OF U^{238}

the sample. If a sample has many closely spaced resonances, these resonances are spread out and made less pronounced by the Doppler effect. Hence, neutrons in traversing a sample are not strongly absorbed by any one resonance.

P-WAVE CONTRIBUTIONS TO THE CROSS SECTION

Neutrons of angular momentum $\ell = 1$ do not show their effects on the cross sections until we reach the kev region. Therefore, one very important aspect of this work is to show where and to what degree the p-wave neutrons are effective.

For neutrons with $\ell > 0$, an additional effective potential is introduced into the Schrödinger wave equation. This potential causes an effective barrier penetration factor which is dependent upon the angular momentum of the incident neutron. The values of the penetration factor for angular momentum of 0 and 1 are given as (F1):

$$v_0 = 1 \qquad\qquad v_1 = \frac{x^2}{1 + x^2}$$

where $x = k a$, k is the wave number of the incident neutron and is equal to $2\pi/\lambda$, and a is the nuclear radius, which is given by:

$$a = 1.45 \times 10^{-13} A^{1/3}$$

The barrier penetration factor, v_ℓ, influences the neutron width in the following way:

$$(\Gamma_n)_\ell = v_\ell \Gamma_n^0 \sqrt{E_n}$$

For neutrons of angular momentum $\ell = 1$, we have

$$\Gamma_n = \Gamma_n^0 \sqrt{E_n} \frac{x^2}{1 + x^2}$$

Its effect on the neutron width is to make

$$(\Gamma_n)_{\ell=0} \gg (\Gamma_n)_{\ell=1}$$

At the beginning of this chapter, we defined the statistical weight factor as $g = (2\ell + 1)g' = \frac{1}{2}\frac{2J + 1}{2I + 1}$ For $\ell = 0$ neutrons $g = g'$ and g is double valued, because J can have two values when $\ell = 0$. The experimental resonance parameters $\overline{D}$, $\overline{\Gamma_\gamma}$ and $\overline{\Gamma_n^0}$ are assumed to be equal for both J values ($\ell = 0$). With this assumption, we can sum the cross section equations over the J values. This sum for $\ell = 0$ neutrons makes $\sum_J g = \sum_J g' = 1$. Similarly, for $\ell = 1$ neutrons, J becomes multi-valued. But if we assume that the resonance parameters are the same for each J arising from a given ℓ, we can again perform a summation over the J values which makes $\sum_J g = 1$. In this case, we have $\sum_J g = \sum_J (2\ell + 1)g' = 3$. Therefore, the effect on the cross section equations due to the summation over the J values arising from a particular ℓ is to multiply the cross section equations by the term $(2\ell + 1)$. Because the total capture cross section is a sum of the partial capture cross sections due to neutrons of different angular momenta, the cross section equations must be summed over all possible ℓ values.

The parameters for p-wave neutrons have not been found experimentally, but the shape of the average capture cross section in the kev region can be found. Therefore, we are at liberty to adjust the parameters for p-wave neutrons in such a way as to obtain a theoretical fit to the experimental curve. The cross section equations 2.9 and 2.13 contain only the ratios of the parameters. Therefore, we can consider the two

ratios, $\left(\Gamma_\gamma / \bar{D}\right)_{\ell=1}$ and $\left(\Gamma_\gamma / \bar{\Gamma}_n^0\right)_{\ell=1}$, as two new parameters.

In calculating the cross section due to p-wave neutrons, we made the following assumptions as a first approximation for the parameters in equations 2.9 and 2.13.

$$\left(\frac{\Gamma_\gamma}{D}\right)_{\ell=1} = \left(\frac{\Gamma_\gamma}{D}\right)_{\ell=0}$$

$$\left(\frac{\Gamma_\gamma}{\bar{\Gamma}_n^0}\right)_{\ell=1} = \left(\frac{\Gamma_\gamma}{\bar{\Gamma}_n^0}\right)_{\ell=0}$$

If a fit could not be obtained, the ratio $(\Gamma_\gamma/\bar{\Gamma}_n^0)_{\ell=1}$ was varied since this ratio was the one most likely to differ.

Fig. 2 shows the p-wave contributions from the various distribution functions. These curves were calculated using the same parameters for each distribution function.

A summary of the complete capture cross section equations follows:

For Distribution e^{-y}

$$\left(\bar{\sigma}_a\right) = \sum_\ell (2\ell+1)\,\frac{\pi}{2}\left(\frac{2.6\times10^6}{E_n}\right)\frac{\Gamma_\gamma}{D}\left[1 - x_0 e^{x_0}\int_{x_0}^{\infty}\frac{e^{-x}}{x}dx\right] \qquad 2.14$$

where $x_0 = \dfrac{\Gamma_\gamma}{v_\ell \bar{\Gamma}_n \sqrt{E_n}}$

For s-wave neutrons, $\ell = 0$, $v_0 = 1$ and $\sum_J g' = 1$

For p-wave neutrons, $\ell = 1$; $v_1 = \dfrac{x^2}{1 + x^2}$ and $\sum_J g' = 1$

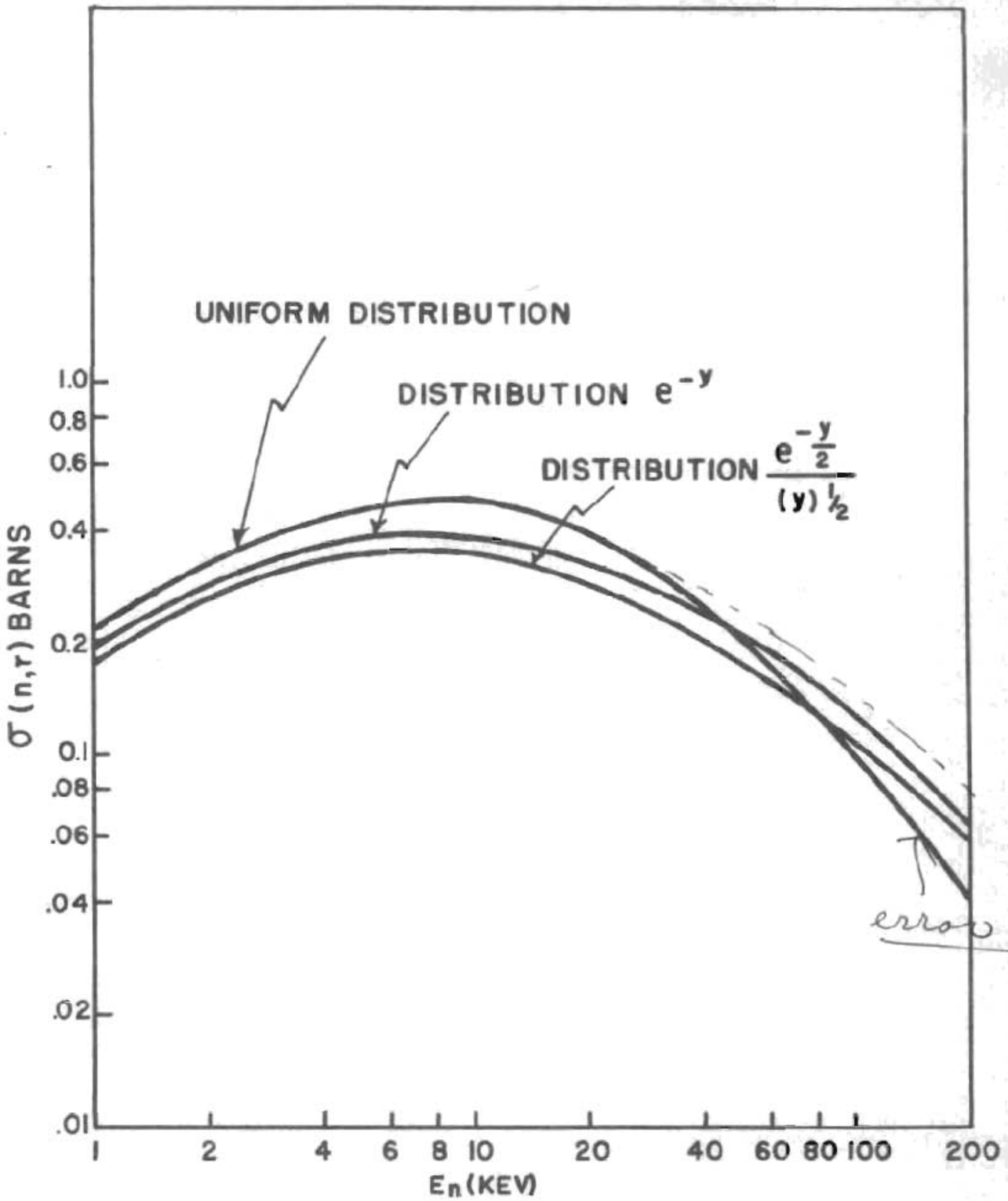

FIG 2 P-WAVE CONTRIBUTION TO THE CAPTURE CROSS SECTION OF U^{238}

For Distribution $e^{-W^2}/(y)^{\frac{1}{2}}$

$$(\overline{\sigma_a}) = \sum_{\ell} (2\ell+1)\,\frac{\pi}{2}\left(\frac{2.6\times10^{+4}}{E_m}\right)\frac{\Gamma_\nu}{D}\left[1-\sqrt{b\pi}\,e^{b}\left(1-\frac{2}{\sqrt{\pi}}\int_0^{\sqrt{b}} e^{-t^2}\,dt\right)\right] \qquad 2.15$$

where $b = \dfrac{\Gamma_\nu}{v_\ell\, 2\sqrt{n^0}\sqrt{E_n}}$

s-wave neutrons, $\ell = 0$, $v_0 = 1$ and $\sum_J g' = 1$

p-wave neutrons, $\ell = 1$, $v_1 = \dfrac{x^2}{1+x^2}$ and $\sum_J g' = 1$

CHAPTER III

EXPERIMENTAL PROCEDURE

Neutrons in this experiment were produced from the $Li^7(p,n)Be^7$ reaction. Protons, produced by the Van de Graaff at Duke University were first sent through a magnetic deflection system then through an electrostatic analyzer. The beam from the electrostatic analyzer was in the neighborhood of 10 micro-amperes. The beam resolution was equal to one part in fifteen hundred for the low energy points and approximately one part in one thousand for the high energy points. The analyzed beam bombarded a thin lithium target to produce monochromatic neutrons. The lithium targets were evaporated on a circular platinum foil with a diameter of 0.75" and thickness of 0.002". The thickness of the lithium target was approximated from the forward threshold curve for the $Li^7(p,n)Be^7$ reaction. All targets used in this experiment were two to three kev thick, and for each run a new target was evaporated and put into place immediately before the run began. The platinum cap was soldered inside a 3/4" silver tube approximately $\frac{1}{2}$" from the end. The platinum cap had to be inset because 90° neutrons were used throughout this experiment, and the target area was cooled by a distilled water spray. The samples were placed at 90° to the proton beam and, therefore, neutrons had to go through the sides of the silver tube in order to reach the samples. The silver tube was 0.005" thick; in the region 10 kev to 300 kev, the total cross section for Ag is flat and equal to 8 barns. Thus,

neutrons in this region will have a 99.7% transmission through the silver tube. This is true only for very closely spaced resonances where the Doppler spread is $\lesssim$ 10 ev $\lesssim$ D.

The samples of Ag and In were metal foil 0.005" thick and 1/8" wide. These samples were put inside a Cd shield and wrapped around the outside of the Ag tube. The Cd shield was necessary in order to keep thermal neutrons from reaching the samples and being absorbed. The U sample was also in the form of a ring, shielded by Cd and fitted into place. The angle subtended by the samples in a plane normal to the proton beam was 2π radians. Consequently, all the neutrons that left the lithium target at a given energy were intercepted by the samples. The angle subtended by the samples in the plane of the proton beam was about 15°. The total solid angle subtended by the sample was 0.125 steradians. Due to the width of the samples, the energy resolution of the neutrons was not sharp; for instance, for 20 kev neutrons at 90° the spread in energy was 10 kev. The nuclear levels for Ag, In and U in the kev region are much too close to be resolved, and this experiment was designed only to measure the average capture cross section over a number of neighboring resonances.

The energy of the protons was controlled by the potential applied to the electrostatic analyzer, and the energy of the neutrons at 90° was calculated by the method described by Hanson, et al (H2). The neutron forward threshold was taken before, during and after each run. In this way, we were able to keep a close check on the neutron energy during a particular run. If changes in the threshold appeared, appropriate

corrections were made to the neutron energy.

During an exposure, the proton current and the neutron yield were both monitored. The relative neutron yield at 90° was measured with a BF_3 long counter. This counter was constructed following the original Hanson-McKibben (H1) model. The chief difference is that our BF_3 counter is at a pressure of 100 Cm. Hg, while McKibben's counter was at a pressure of 25 Cm. Hg. Also, our counter wall was made of Al instead of brass.

All induced activities were normalized against the BF_3 counting rate. Therefore, it was essential to know whether or not the efficiency of the long counter varied with neutron energy. An experiment was performed in the Summer of 1955 by Rohrer (R2) in which he measured the total cross section of B^{10} in the region 3 kev to 100 kev. The total cross section of normal Boron has been measured (S4) from 0.001 ev to 100 ev. After subtracting a small contribution due to the scattering cross section, the capture cross section was found to follow the 1/v law. This capture cross section is due primarily to B^{10} and is given by:

$$\sigma(n,\gamma) = \frac{\text{constant}}{\sqrt{E}} \qquad 3.1$$

This equation was assumed to be true to at least 100 kev, and the $\sigma(n,\gamma)$ (equation 3.1) for B^{10} was subtracted from each point of the total cross section found by Rohrer. The difference should be the scattering cross section. These curves are shown in Fig. 3. Above 70 kev (not shown), the scattering cross section appeared to increase. The average scattering cross section over the region 3 kev to 70 kev was found to be

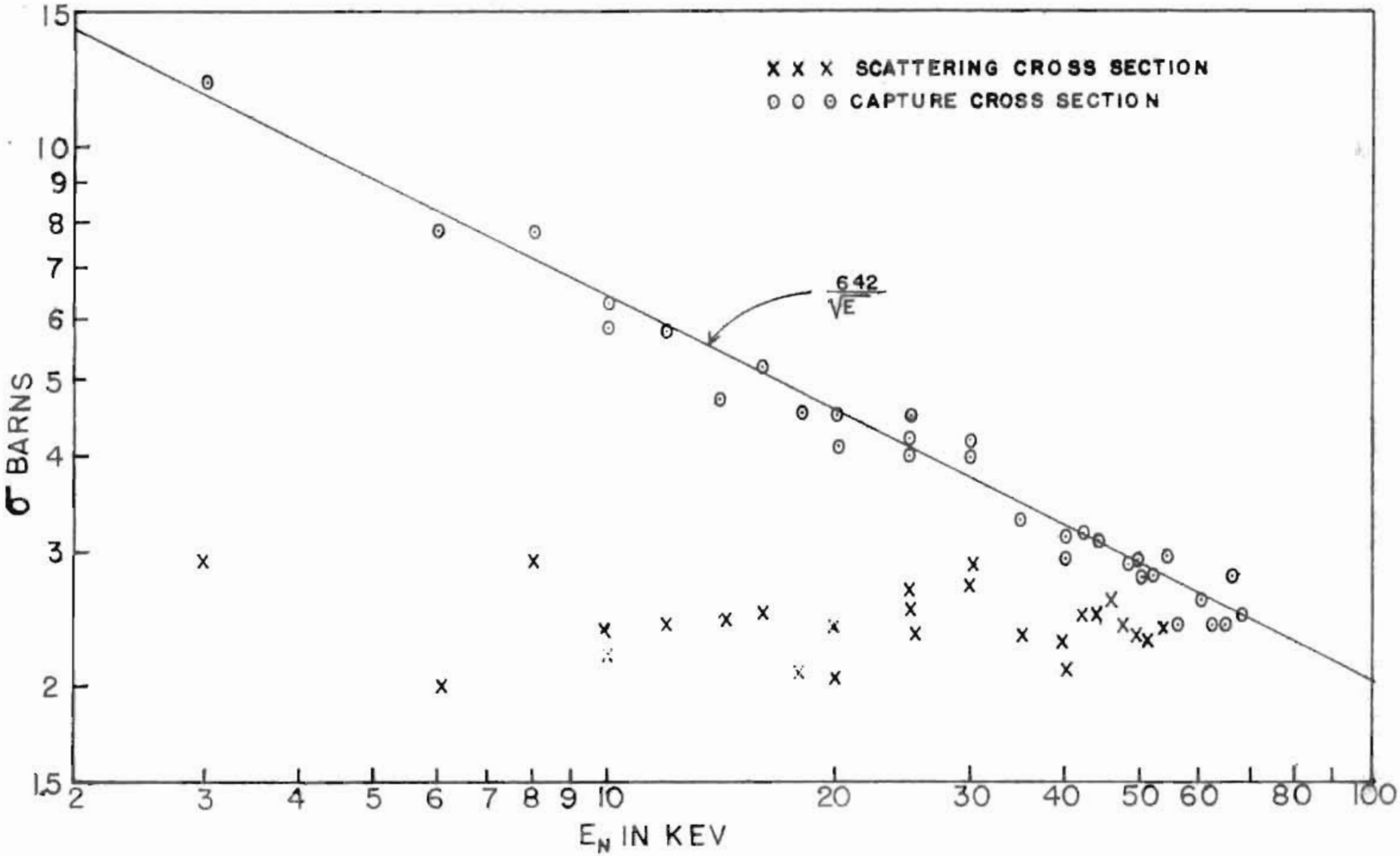

FIG 3 CAPTURE AND SCATTERING CROSS SECTION OF BORON 10

2.42 barns. This agreed well with the value of 2.43 barns (H8) reported for energies up to 20 kev. Therefore, it was reasonable to assume that $\sigma(n,\gamma)$ goes as 1/v at least up to 70 kev. The points which cluster about the calculated $\sigma(n,\gamma)$ curve were found by subtracting the average scattering cross section of 2.42 barns from the total cross section. This will give one some idea of the point scatter encountered in this experiment.

Since it has been shown that $\sigma(n,\gamma)$ for B^{10} follows the 1/v law up to 70 kev, the "flatness of response" of the long counter was tested in the following manner. A bare BF_3 counter surrounded by Cd was placed at 90° to the proton beam, and its counting rate was observed as a function of neutron energy. The bare BF_3 counter was placed approximately 4" away from the target area. At each corresponding energy and at the same angle, the neutron flux was monitored by the long counter. Both counting rates were corrected for background due to scattered neutrons. These background rates were obtained by putting a 4" paraffin wedge between the target and the bare BF_3 counter and by putting a 7" truncated cone of paraffin between the target and the long counter. This method of getting the background rate will be discussed in greater detail in a later section.

If the counting rate of the bare BF_3 counter followed the 1/v law and if the efficiency of the long counter was constant, the ratio $\frac{BF_3 \text{ counting rate}}{\text{long counter counting rate}}$ at each energy would go as 1/v. The results of this experiment are shown in Fig. 4. The solid curve is given by equation 3.1, and the experimental points consist of three separate runs

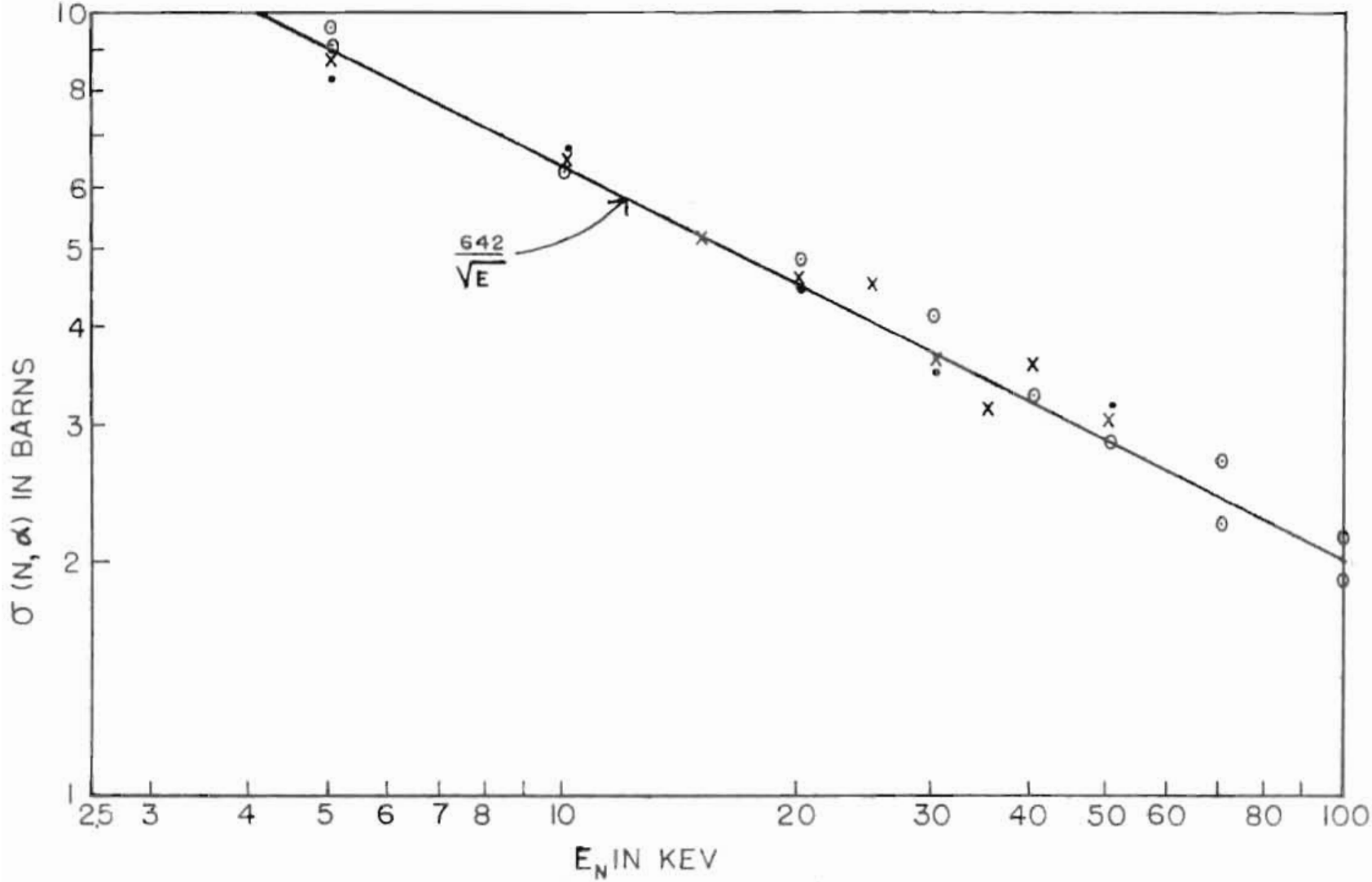

FIG. 4 PTS. FROM THE RATIO 3.2 NORMALIZED TO THE CAPTURE CROSS SECTION OF BORON 10

taken approximately two weeks apart. This graph shows that to 70 kev, the long counter was constant in efficiency within 10%. An attempt was made in two of the runs to extend the experimental points to 300 kev, but it was found that beyond 100 kev, the room background was several times larger than the counting rate of the bare BF_3 counter. This was due to the fact that the capture cross section of the BF_3 counter decreases as the neutron energy is increased. Because the ratio of the rates of the bare BF_3 counter to the long counter followed the 1/v law well into the 100 kev region, the total cross section above 70 kev (Al) for B^{10} indicates an increase in the scattering cross section.

One important correction had to be made to the counting rate of the long counter: this was the background due to target neutrons scattered from the walls, floor and the target backing, and to stray neutrons originating from various points along the proton beam tube. Some samples were activated at 3 kev; and at this energy, the 90° neutron yield was less than the room background. Hence, background became an important factor. In order to reduce room background as much as possible, all material not essential to the experiment was removed from the target area. Also, an extension was put on the proton beam tube so that the lithium target was extended out over the pit in the Van de Graaff room. The pit is approximately 4 feet lower than the surrounding floor. This put the lithium target approximately 8 feet from the bottom of the pit.

The correction due to stray neutrons and to neutrons scattered from the walls and floor was found by inserting a truncated cone of paraffin between the target and the long counter. The cone was cut in

such a way that neutrons produced at the target could not "see" the long counter. The small end of the truncated cone was placed 2½" away from the target; and if this end were completed, the apex of the cone would be at the neutron source. The truncated cone had a total length of 7". The mean free path of a neutron in the kev region is about 0.9 Cm (B1) for paraffin. Therefore, all direct neutrons to the long counter were assumed to have been scattered. The long counter was always kept at a distance of 37" from the target. For each run and for each energy, the long counter rate for 80 μCoulombs was taken with the cone inserted in position and with the cone removed. The difference between the two rates then gave a measure of the direct neutrons.

To measure the neutrons scattered from the target backing was a little more difficult and could only be done in an indirect manner. A sample was put in position, and the proton energy was reduced so that neutrons from the Li^7 (p,n) Be^7 reaction would only be produced below 80°. Since the sample was at 90°, there were no direct neutrons from the target. Those neutrons that seemed to be coming from the target and detected by the 90° long counter could only be due to neutrons scattered towards the sample by the target backing. Under these conditions, any activity observed in the sample must be due to neutrons scattered from the target backing. This correction was in the neighborhood of 2 to 3 per cent.

The pulses from the long counter were fed to a preamplifier, an amplifier, then to a single channel analyzer and finally to a scaler. The channel width of the analyzer was opened to the maximum value, and

bias curves were run on the long counter. This was necessary because of the high gamma ray activity from the Li^7 (p,n) Be^7 reaction. Williamson (w3) has shown that this activity increases with proton energy. With a low bias setting, the long counter was found to be sensitive to gamma rays. Hence, with such a setting, one would be counting gamma rays as well as neutrons. Therefore, the bias on the long counter was set high enough to give only counts due to neutrons. It was important that no gamma rays be counted by the monitor, because Williamson's data showed that the gamma ray intensity did not increase with energy at the same rate as the neutron yield increased. If this were not the case, then an error would have been introduced in the experiment, because the induced activities in the samples were all normalized to the number of counts registered by the long counter.

PROTON CURRENT MONITOR

It has been stated previously that the proton current was monitored. It should also be stated that the monitored beam was in the form of a permanent record. A resistor was placed between the target area and ground. The voltage drop across the resistor, due to the proton current, was fed to a Leeds and Northrop recorder. This recorder had a full scale deflection for a voltage of ten milli-volts. Therefore, with a resistance of 1000 ohms and a proton current below 10 micro-amperes, the recorder could be read directly in micro-amperes.

The permanent record of the beam current served a dual purpose. First, for a particular exposure, the total charge in micro-ampere

minutes was found from the chart. The total count of the neutron monitor for the same exposure was then divided by this total charge to give the neutron rate per micro-ampere minute. This number, number of counts per unit charge, was used as a normalizing factor for each exposure. Second, because the activated samples decay during an exposure, the total effective current at the end of an exposure had to be calculated. This was done by subdividing the chart for a complete exposure into intervals small compared to the half-life of the induced activity. The decay of the induced activity is given by the expression:

$$N = No(1 - e^{-\lambda t}) \qquad 3.2$$

N = number of nuclei that have decayed

No = number of radioactive nuclei present at t = 0

λ = decay constant and is equal to 0.693/T where T is equal to the half-life

In this experiment, there was a continuous generation of nuclei that may undergo decay. Therefore, the average value of the current over each sub-interval of the total exposure time was multiplied by the appropriate factor $e^{-\lambda t}$, where t is the time from the end of the exposure. For example, suppose we activate a sample which has a half-life of 60 minutes, and the exposure time is also 60 minutes. We then divide the total time into intervals of 1 minute and multiply the average current over each one minute by $e^{-\lambda t}$. In this case, if we had a current of 10 micro-amperes throughout the exposure, then the first minute of exposure would be multiplied by $e^{-\frac{.693}{60}60}$ giving an effective current for this interval of 5 micro-amperes at the end of the exposure. The weighted currents over

each sub-interval were then added to give a total effective current. The total weighted current can be expressed as

$$I = \sum_n I_n e^{-\frac{.693}{T} t_n} \qquad 3.3$$

In = the average current over the n^{th} interval

tn = the average time of the n^{th} interval from the end of the exposure

T = the half-life of the induced activity

All induced activities were normalized with respect to this weighted current.

MEASURE OF INDUCED ACTIVITIES

The particulars for each element studied will be given in Chapter V. At this point, only a general discussion of the treatment of activated samples will be given.

As stated earlier, the samples were in the form of rings 0.8" in diameter. These rings were put in position at a mean angle of 90° to the proton beam. The exposure time for each energy of the element being studied was kept constant once it was determined from preliminary runs. The governing factors on the exposure time were:

(a) the half-life of the induced activity being studied;

(b) the neutron capture cross section of the element being studied;

(c) background of the beta counter as compared to the counting rate of the induced activity.

To get the maximum induced activity, one should expose each sample until saturation occurs. For half-lives greater than 30 minutes, this is not practical because of the length of time involved in each exposure. In this experiment, the exposure time was considered sufficient if the induced activity rate at the end of the exposure was approximately 10 times greater than the background of the beta counter.

Once the sample was activated, it was taken off the proton beam tube and placed around a beta counter. Counting of the beta activity always began one minute after the end of the exposure. The pulses from the beta tube were amplified and fed to a scaler. The scaler was allowed to run continuously, and the differential decay curve was obtained by reading the scaler for periods that were short compared to the half-life of the activity.

Equation 3.2 gives us the number of nuclei that have decayed up to time t. Therefore, $N_t = No(1 - e^{-\lambda t})$

After a time $t + \Delta t$ we have:

$$N_{t+\Delta t} = No(1 - e^{-\lambda(t+\Delta t)})$$

By subtracting these two equations, we get the number of decays in time Δt.

$$\triangle N = No\, e^{-\lambda t}(1 - e^{-\lambda \Delta t}) \qquad 3.4$$

If Δt is kept constant, then $1 - e^{-\lambda \Delta t}$ is a constant, and a plot of the $\log \Delta N$ versus time gives a straight line whose slope is λ .

The counting rate of the beta tube was only a relative one. This was due to the fact that by putting the activated samples around the outside of a beta tube, a counting geometry of only 2π was obtained. Also, there was self-absorption of the betas because of the finite thickness of

the samples. All activated samples had the same thickness and were placed in the same position on the beta tube. Hence, all decay curves of a particular element were proportional to the actual decay curve with the same proportionality constant.

Once the decay curves were obtained, they were extrapolated back to zero time to give the beta decay rate per minute at the end of the exposure. This number was called the beta yield at zero time. For a particular element, the mass of each sample differed slightly, and this correction was made by normalizing the beta yield to the mass.

For an element of given foil thickness, the beta activity was proportional to the mass of the sample, and the mass of the sample was proportional to the width. Relative capture cross section curves were plotted using the width in one case and the mass in another. No difference in the shape of the relative cross section curves could be detected.

CHAPTER IV

BACKGROUND TECHNIQUES

In the Summer of 1954, a series of experiments (C1) were performed at Duke University with two objectives in mind:

(a) to reduce to a minimum the background of a single thin wall beta counter; and

(b) to determine the source of these background counts.

The counter used was an R.C.L. counter, Model 10. This counter had a wall thickness of approximately 35 mgm.$Cm.^{-2}$ glass and an effective counting volume of 1.235 cubic inches (3" x 3/4"). This single beta counter was surrounded by a group of Cu cosmic ray counters which were in anti-coincidence with the beta counter. This assembly of counters was then placed inside an "oven" of lead and steel to shield the counters from the soft component of cosmic rays. The counting rate of the thin wall beta tube was found to be about 5.5 c.p.m.

This counting rate was the lowest achieved and the source of background was attributed to:

(a) spurious counts from high potential points on the wire;

(b) alpha particle contamination in the material from which the beta counter was made; and

(c) inefficiency of the anti-coincidence ring against all cosmic rays.

Shortly after the above work was completed, Dr. E. D. Palmatier and the author designed and built a thin wall beta counter. The counter was made of Al with wall thickness of 37 mgm. $Cm.^{-2}$ and an effective counting volume of 1.473 cubic inches (0.688" x 4"). The center wire was 5 mils tungsten, and great care was taken to flash the wire in order to remove any foreign material. In this way, we hoped to lessen the spurious counts from high potential points. In order to remove counts from alpha emitting materials which might have been in the Al, the inside of the counter was coated with collodian of approximately 0.0005" thickness. The filling gas was 99% He and 1% polyatomic gasses. The tube was filled to one atmosphere pressure. The plateau of this beta tube was exceptionally good --- being greater than 360 volts long with very little or no rise as voltage on the tube was increased. Under identical conditions, the glass beta tube gave a counting rate of 7.3 $\pm$ 0.2 c.p.m. and the Al beta tube gave a counting rate of 4.41 $\pm$ 0.07 c.p.m. The Al beta tube has approximately 20% more volume, and when compared to the volume of the glass beta tube, its counting rate is 3.5 c.p.m.

It was concluded at this point that the only way to decrease the background rate was either to cut down the effective volume or design a new set up in which we could eliminate sources of the background absolutely. The latter course of action was followed.

A multi-tube counter was designed from which we eliminated the suspected sources of background by coincidence counting and yet effectively had a thin wall beta counter. At the same time, we decided to improve

our counting geometry by making this counter a 4 π counter. When using a single counter, one usually has a counting geometry of 2 π unless it is a flow type counter where one can introduce a sample inside the counter.

Two cross sectional views of the multi-counter are given in Fig. 5 and Fig. 6. The one inch center hole is open to the atmosphere, and the sample to be counted can be introduced into this volume. The counter was made of Al with the inside wall of 0.004" thickness. The wall thickness between the two rings of counters is 0.002". Therefore, to get a coincidence count, an electron must traverse 0.006 inches of Al, or 41 mgm. $Cm.^{-2}$ From range energy curves for electrons (M2), an electron of 100 kev can penetrate this thickness. This is to be compared to the energy which an electron needs to penetrate the wall thickness of a glass beta tube. The beta tube wall thickness is 35 mgm. $Cm.^{-2}$, and the corresponding energy of the penetrating electron is 175 kev.

Since we now demanded a two-fold coincidence for a count to register, we immediately saw that counts due to spurious events were eliminated. Furthermore, the 0.002" wall thickness between the two rings is enough to stop all alpha particles decaying from contaminating elements in the Al. Therefore, two sources of background were eliminated.

The multi-counter consists of fourteen G-M counters; six in the inside ring (A ring), and eight in the outside ring (B ring). The center wires are 3 mil Molybdenum. Molybdenum wire was used here because it retains its flexibility after it has been flashed. To reduce the amount of material inside the counter, the radial sides were made up of 5 mil

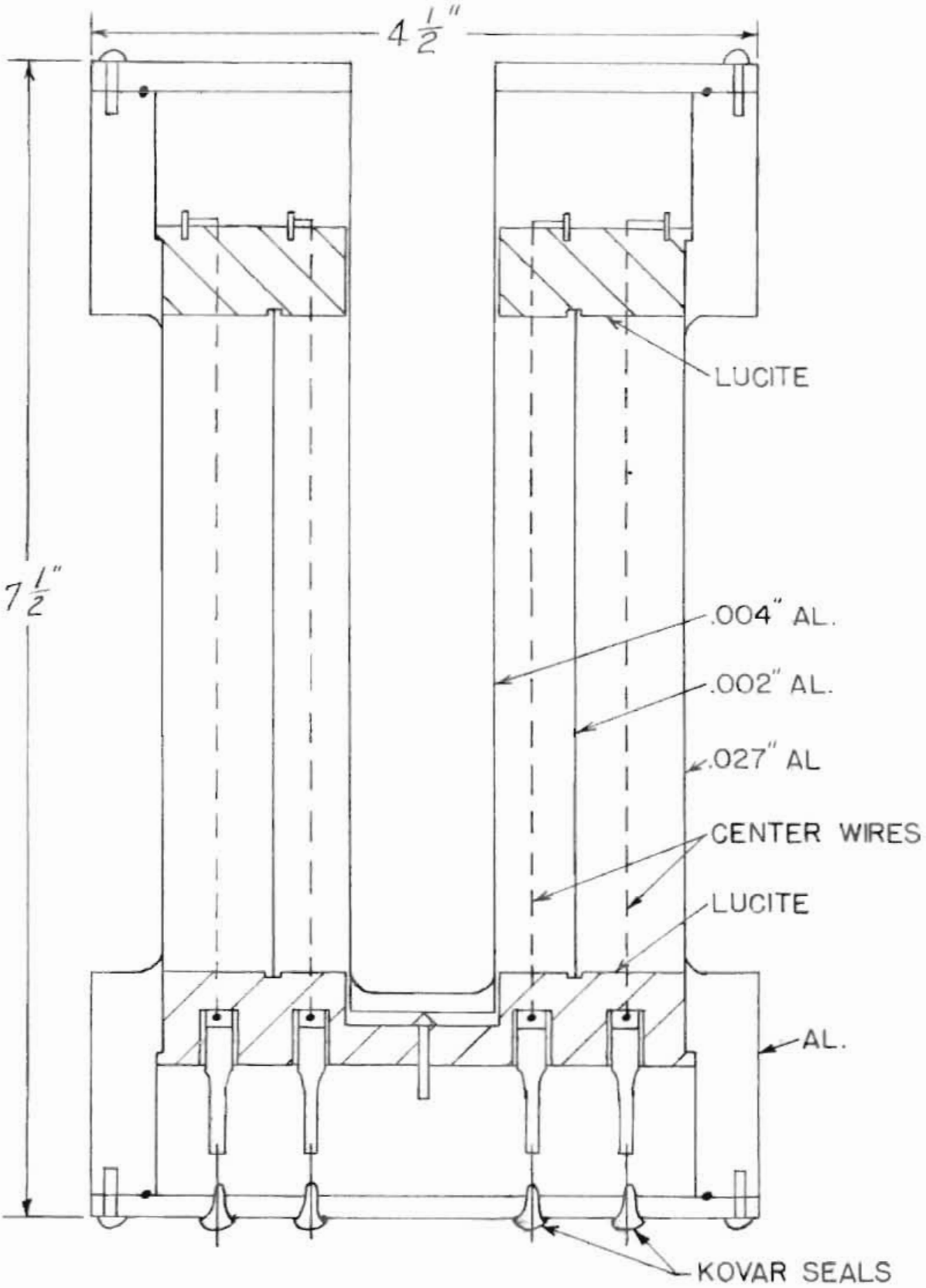

FIG. 5 LONGITUDINAL SECTION OF MULTI-COUNTER

SCALE: 1:1

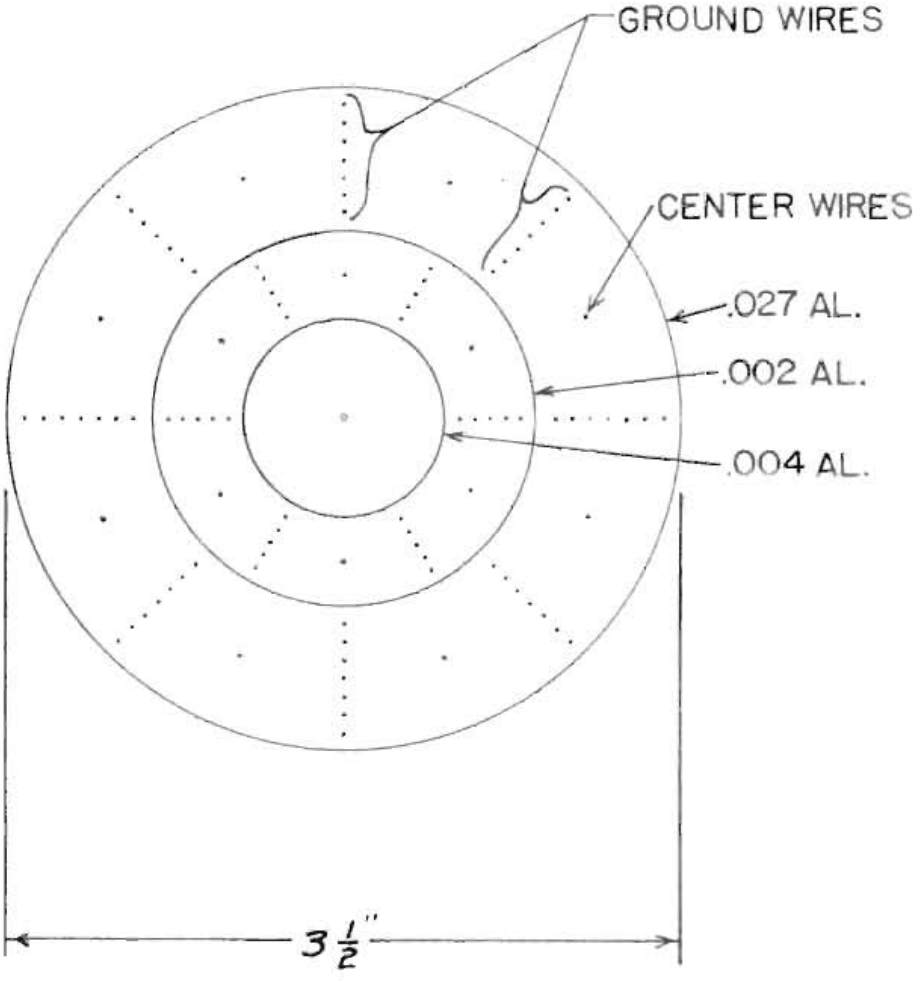

FIG. 6 TRANSVERSE SECTION OF MULTI-COUNTER

tungsten wires strung back and forth between the lucite end pieces. These wires all went to a common ground. The outermost wall was 0.027" thick and the effective counting volume was 45.8 cm^3 ($3\frac{1}{2}$" x $4\frac{1}{2}$"). The plateaus of individual counters were taken and found to be 150 volts or greater for all counters. In order to insure that Ring A was completely isolated from Ring B, the lucite end pieces were painted black on the inside. A series of experiments were performed to demonstrate that a discharge in Ring A did not in any way effect or cause a discharge in Ring B or vice versa.

A block diagram of the circuit is shown in Fig. 7. The "line driver" takes a G-M pulse and shapes it into a positive square of 3 micro-seconds duration. The resolving time of the coincidence circuit (J2) is 2 micro-seconds. The anti-coincidence circuit also has a "line driver" which is followed by a Schmidt circuit. The Schmidt circuit takes the positive square wave of the line driver and puts out a negative pulse whose front face falls to a minimum in approximately 1 to 2 micro-seconds. this pulse can be varied from 100 micro-seconds to 700 micro-seconds. The Schmidt circuit pulse is then fed onto a grid of the mixer tube. The coincidence pulse is delayed 8 micro-seconds to insure cutoff of the mixer tube when an anti-coincidence and a coincidence pulse start from the G-M counters at the same time.

If we designate by:

A - the counting rate of the A Ring

B - the counting rate of the B Ring

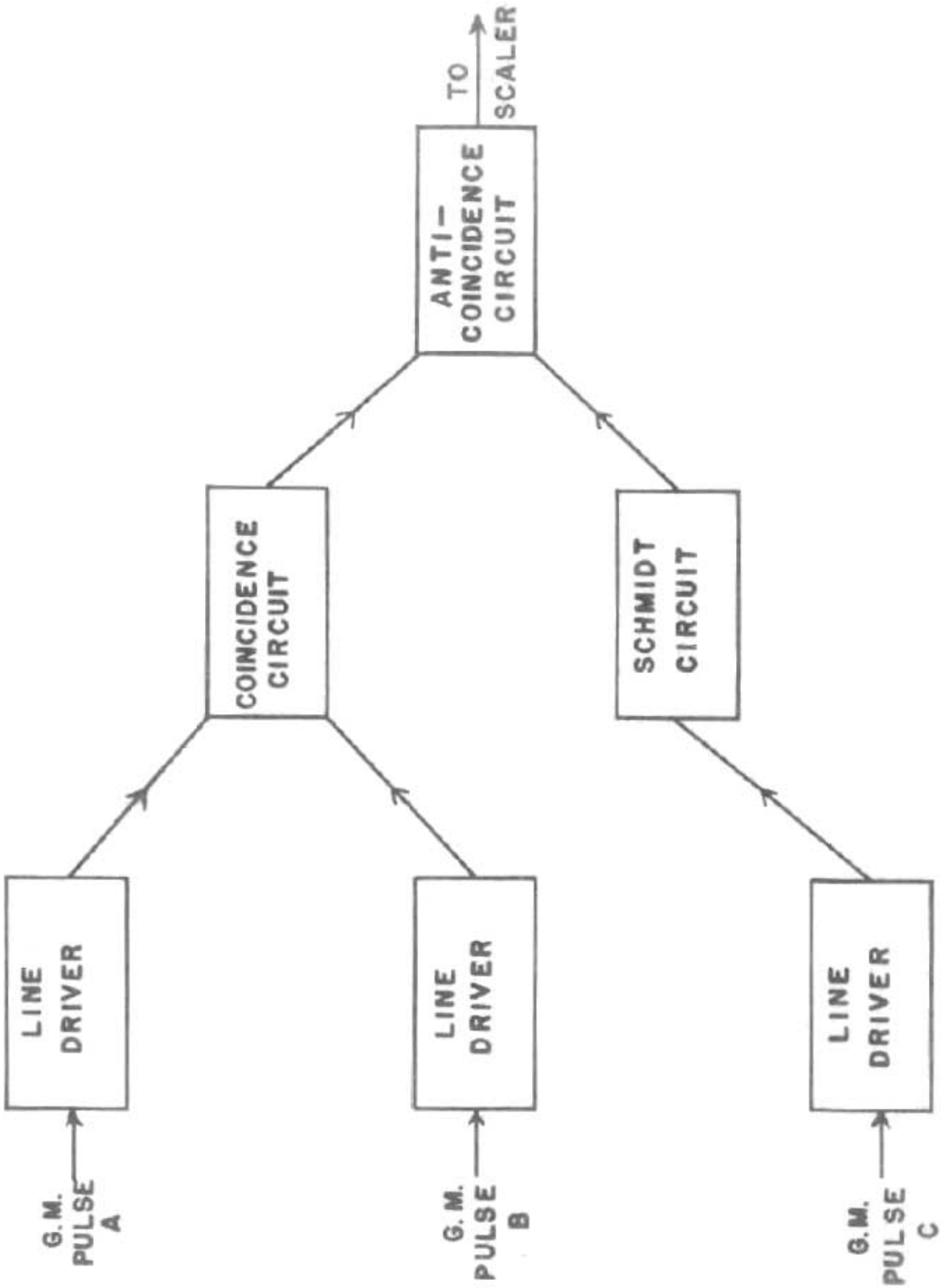

FIG 7 BLOCK DIAGRAM OF COUNTING CIRCUITS

C - the counting rate of the anti-coincidence ring

then, AB equals the coincidence rate of the A and B rings, and AB-C equals the coincidence counting rate minus those pulses which are common to A, B and C. This latter is the counting rate we hoped to eliminate.

The C Ring consisted of 10 R.C.L. cosmic ray counters Model 53-40, which formed a complete ring around the multi beta counter. To eliminate the possibility of a charged particle passing between two counters of the C Ring, ten 1" x 20" Cu cosmic ray counters were used to fill these spaces. Under these conditions, it was believed that the C Ring would detect with 100% efficiency any charged particle penetrating the ring. The anti-coincidence pulse was adjusted so it would last for 450 micro-seconds. This was approximately equal to the time for one of the C counters to recover after it had fired.

The multi-beta tube, with its "guard ring" of 20 counters, was then placed in the "oven" of lead and steel, the steel being innermost to cut out decay particles from the lead. The "oven" was approximately 8" thick on the sides and 10" thick on top. This was enough material to eliminate the soft component of cosmic rays.

With the set up as described above, the AB-C rate was found to be 20 c.p.m. The volume of the A Ring was 7.3 times greater than the volume of a single glass beta counter. So on a volume-for-volume comparison, the background rate for the multi-beta counter with 4π geometry was 2.7 c.p.m. The background rate of a single glass beta counter was found to be 5.5 c.p.m.

An exhaustive study was made in an attempt to find the source of the above background rate. Any and all possible sources were considered:

(a) Pickup in the A channel due to the B channel and vice versa.

(b) Inefficiency of circuits.

(c) Chance coincidence rate between A and B.

(d) Inefficiency of the C Ring against all charged particles.

(e) Secondaries from high energy mesons.

(f) Materialization of γ rays inside the C Ring.

(g) Production of photo and Compton electrons inside C Ring.

(h) Local beta contamination; either on the counter or in the material from which it was constructed.

In order to insure that a coincidence was not due to pickup, all channels were isolated from each other. The circuit efficiency was checked in several ways. One of these experiments simply consisted of feeding the pulses from a G-M tube to all three channels to find out if pulses could sneak through. This experiment, among others, showed the circuits to be 100% efficient.

The rate due to chance coincidence is given by:

$$R = 2\tau N_A N_B \qquad 4.1$$

τ = resolving time of circuits = 2×10^{-6} sec.

N_A = counting rate per sec. of the A Ring

N_B = counting rate per sec. of the B Ring

Even for rates of 1200 c.p.m., R would only be 0.1 c.p.m., which is negligible.

The possible sources (d), (e), (f) and (g) above are in some way related to cosmic rays; and although a great many experiments were performed, no conclusive statements could be made about them as sources for the background rate. We could only say that perhaps these four possible sources contributed a percentage of the observed background rate.

The possibility of local contamination was then vigorously attacked. On the assumption that some radioactive substance had gotten on the outside of the counter, 0.005" was turned off the outside of the counter by a lathe. No appreciable difference was observed in the background counting rate. We next showed that this background was isotropic in nature by observing the coincidence rate between various halves of the multi-counter. For example, the coincidence rate was observed for adjacent halves of the A and B Rings for various angles from the azimuth. The coincidence rate was cut in half and showed no dependence on azimuthal angle. Since the multi-counter consists of fourteen individual counters, any arrangement of counters within the multi-counter could be made. The conclusion from this series of experiments wasthat the observed background rate could be due to local beta activity.

At this point, it was decided that the only way to determine the nature of the observed background was to take the counter far below ground where the cosmic ray intensity would be appreciably reduced. A tungsten mine was found to be in operation at Tungsten, North Carolina.*

---

* The author's thanks are extended to Mr. Sweet, of the Tungsten Mining Corporation for permission to set up the experiment below ground.

The experiment was set up in the mine with identical conditions as in the laboratory, but under 300 feet of solid granite. From the work of Rossi (R4), the meson intensity at this depth is reduced to ½% of the sea level intensity. At this depth, the AB-C rate was identical with the sea level rate, and it was concluded that the observed background rate could not have its origin in cosmic rays. Since the observed background rate was isotropic in nature, it would only be deduced that the background was due to local beta contamination in the material from which the counter was made.

Before this method was abandoned, it was decided to attempt one more experiment in which the A Ring was made of six individual glass beta counters, with the B Ring consisting of 12 glass beta counters. Around these counters was placed an anti-coincidence C Ring. The bundle of counters was again put inside an "oven" of lead and steel, and rates were observed as before. In this case, the AB-C rate was 10 c.p.m. Again, it could only be concluded that a minute amount of beta active material was present in the glass. This beta active material could possibly be K^{40}, which emits a beta ray with maximum energy of 1.36 Mev.

Since the background rate could not be eliminated by the above method, it was decided to return to counting samples by a single beta counter. Two methods were used to count the activated samples, the method used depending upon the amount of activity expected. In the case of the Ag^{107} and U^{238} activation, a high activity was expected and minimum background rates were not essential. The counting arrangement consisted of a

single thin wall beta counter (3" x 3/4") placed inside a lead and steel "pig". No anti-coincidence counters were used. The beta pulses were fed to an amplifier and then to a scaler. The background for this arrangement varied from 30 to 80 c.p.m. The counting for Ag^{107} and U^{238} was done next to the Van de Graaff control panel. The radiation in the Van de Graaff room increases when the machine is turned on and, also, increases with machine energy. Hence, one would expect an increase in the background rate of the beta counter. The background rate was taken for each energy setting in order to subtract the proper background rate for each activation.

The second method of counting induced activity was in a room adjacent to that which housed the Van de Graaff. The wall between the two rooms was approximately two feet thick. In this case, the circuits described for the multi beta counter were used, employing the anti-coincidence circuit and only one channel of the coincidence circuit. Again, a single beta tube (3" x 3/4") was used to count the activated samples. In this case, the multi-counter described in the foregoing paragraphs was used in the place of the anti-coincidence counters. The thin wall beta tube was simply put inside the multi-counter. By using the multi-counter in this way, we had a double ring of anti-coincidence counters around the beta counter. The counters were then placed inside a lead and steel "pig" which cut out the soft component of cosmic rays. The background in this case was reduced to 5 c.p.m. By using this counting arrangement and removing the counting apparatus from the Van de Graaff room, it was found that the machine affected the background rate only

slightly. With the Van de Graaff producing a two Mev proton beam, the background rate was observed to increase by 1 to 2 c.p.m. This second method of counting was used to count the induced activity due to In^{116} which has a half-life of 54 minutes.

CHAPTER V

EXPERIMENTAL CAPTURE CROSS SECTIONS

CAPTURE CROSS SECTION OF Ag^{107}

This sample was normal silver foil with a thickness of 0.005", width of 0.1" and length of 2.5". When Ag^{107} is exposed to neutrons, the following reaction occurs:

$$Ag^{107} + n \rightarrow Ag^{108} + \gamma \qquad 5.1$$

$$Ag^{108} \rightarrow Cd^{108} + \beta^- \qquad 5.2$$

The half-life of Ag^{109} is 2.3 minutes. The exposure time was 10 minutes in all cases, and this produced an activity of 4000 to 8000 c.p.m. The counting of the activity took place in the Van de Graaff room, and the background of the Beta counter depended somewhat on the machine energy. This background varied from 30 c.p.m. for the low energy points to 80 c.p.m. for the high energy points.

Fig. 8 shows three typical decay curves obtained in the activation of silver. The solid line was drawn with the proper slope, and the half-life is indicated. In the preliminary exposures, the decay curves were followed for three to four half-lives in order to find out whether some of the activity was due to foreign substances in the material. The results obtained for silver and also for In and U showed that no foreign materials were activated.

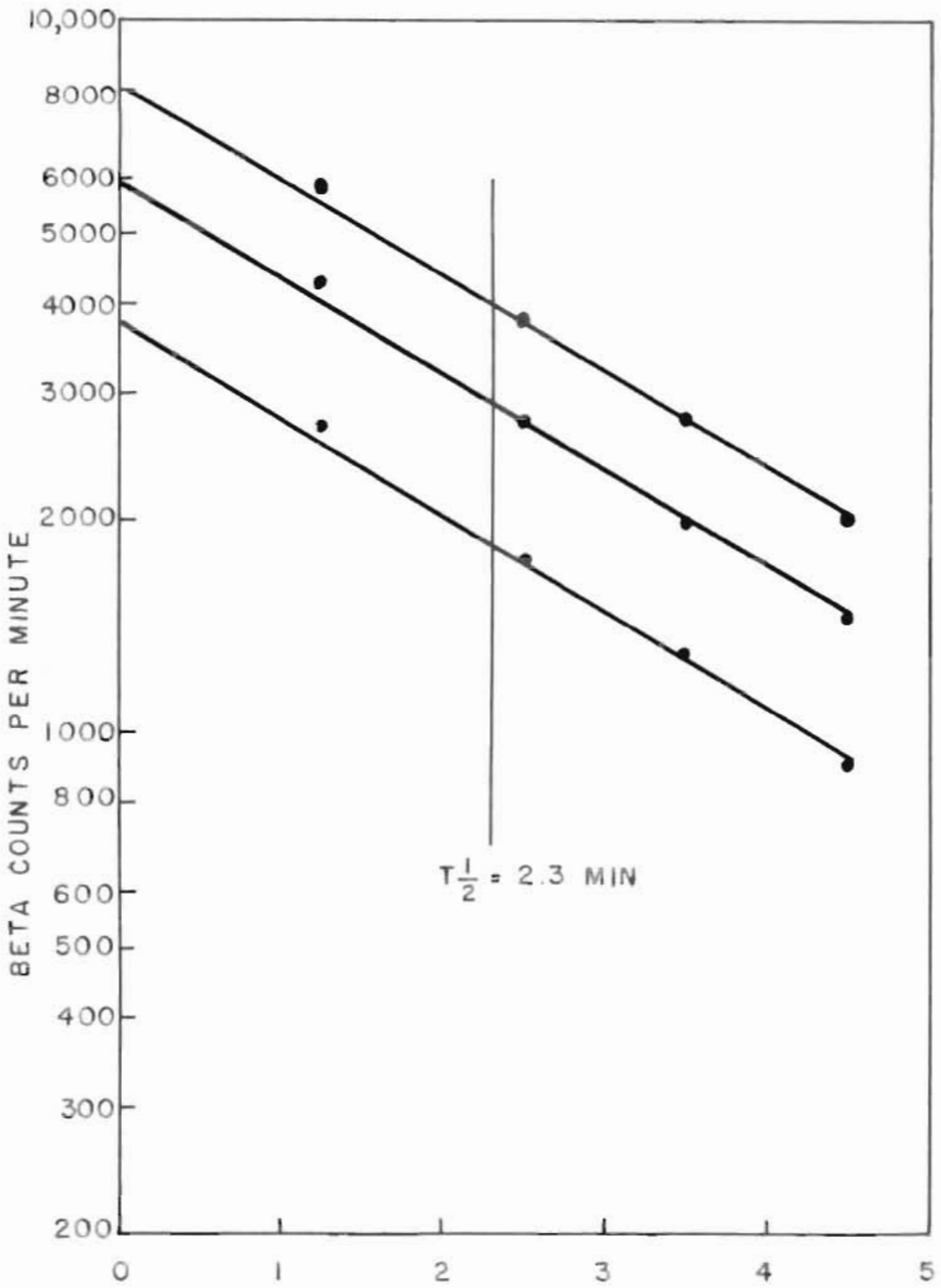

Fig. 8 TYPICAL DECAY CURVES OF Ag^{108}

The other isotope of silver (Ag^{109}), which was present in the sample, was also activated by neutron bombardment. The half-life of the activity due to this isotope is 24 seconds. Since the beta counting did not begin until a minute after the end of the exposure, the beta activity due to this isotope had nearly vanished.

Fifteen points on the average, relative cross section curve were obtained in the region 3 kev to 250 kev. These points are normalized at the high energies to the absolute capture cross section points given by the Los Alamos group (A1). These points are shown in Fig. 9 and Fig. 10 along with the average absolute capture cross section calculated from equations 2.14 and 2.15 (solid line).

The resonance parameters for Ag^{107} are given in a survey article by Carter, et al (C2). These parameters were obtained for neutrons of energy 5 ev to 200 ev and are valid only for $\ell = 0$ neutrons. In our work, they were assumed to be correct for $\ell = 0$ neutrons in the kev region. With present techniques, it is impossible to obtain these parameters directly from the kev region. On the other hand, we can feel reasonably certain that the parameters for $\ell = 0$ are the same in this region since the neutron, after it has entered the nucleus, gets an additional amount of energy of approximately 8 Mev. Hence, the kev region is very close to the ev region on this energy scale.

The calculated curve in Fig. 9 was obtained by using equation 2.14, which gives the average cross section as a function of energy. The curve is a sum of the s-resonance and p-resonance contributions to the capture

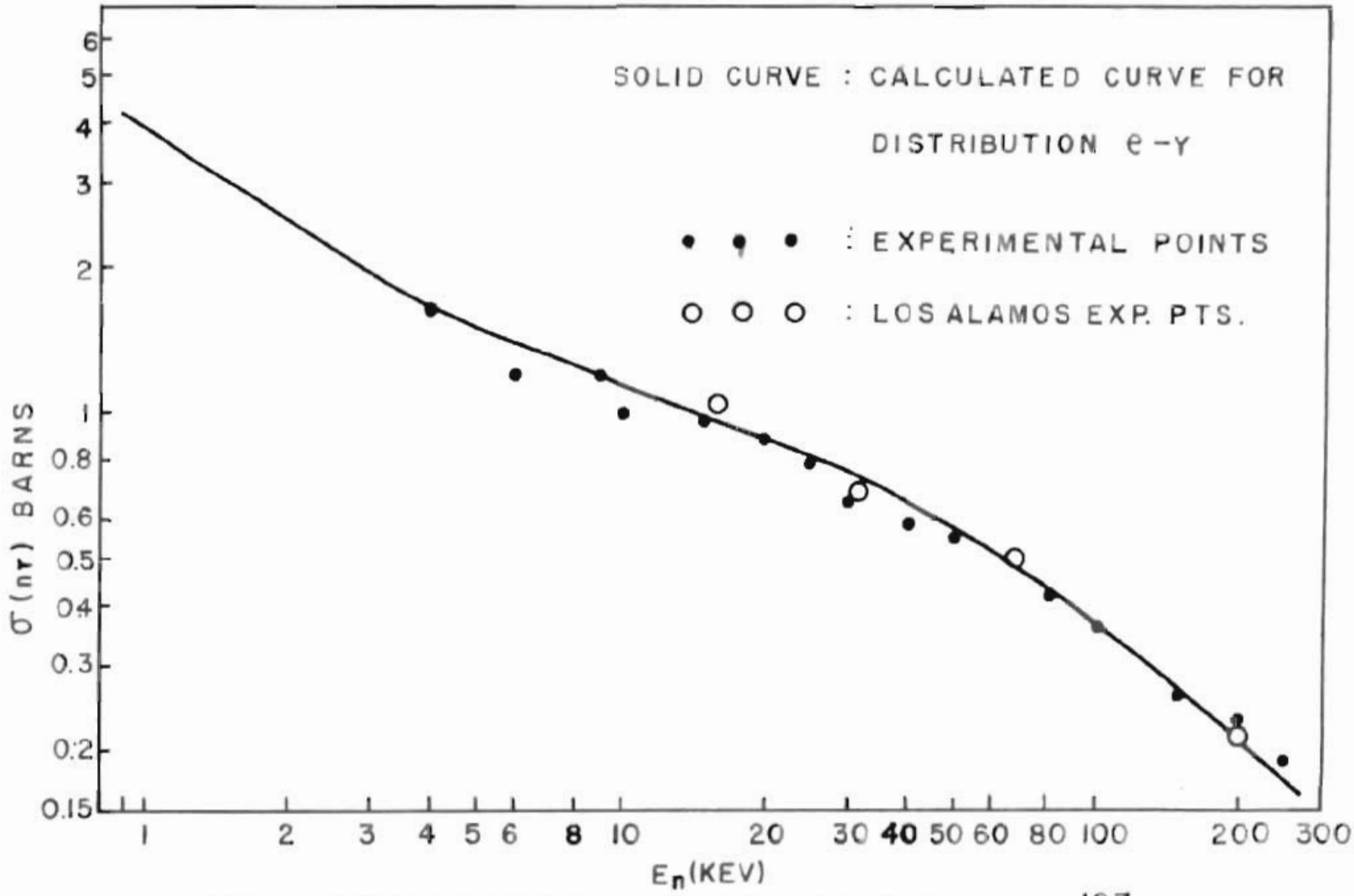

FIG. 9 NEUTRON CAPTURE CROSS SECTION OF Ag^{107}

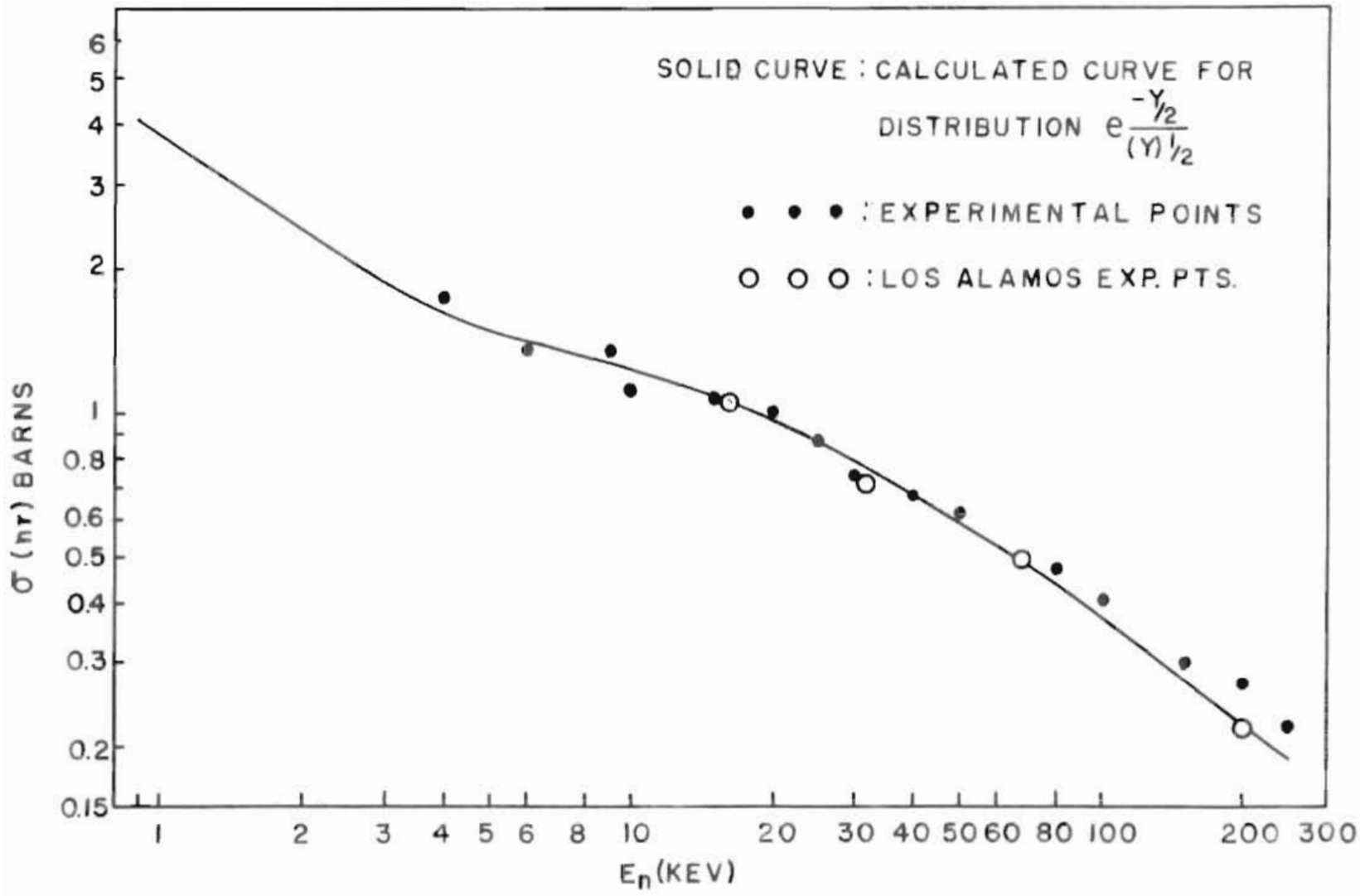

FIG. 10 NEUTRON CAPTURE CROSS SECTION OF Ag^{107}

cross section. The reduced neutron width, Γ_n^0, has been weighted with the distribution function e^{-y}, where $y = \Gamma_n^0/\bar{\Gamma}_n^0$.

The parameters used for neutrons of angular momentum $\ell = 0$ are given by Brookhaven (C2).

$\bar{D} = 40 \pm 10$ ev $\qquad \bar{\Gamma}_n^0/\bar{D} = 0.5 \pm 0.2 \times 10^{-4}$

$\Gamma_\gamma = 0.13$ ev

$\bar{\Gamma}_n^0 = 2.0 \pm 0.9$ mv $\qquad \Gamma_\gamma/\bar{D} = 3.25 \times 10^{-3}$

The parameter most likely to show variation with ℓ is the reduced neutron width, Γ_n^0. As stated in Chapter II, only the ratios, $\Gamma_\gamma/\bar{D}$ and $\Gamma_\gamma/\bar{\Gamma}_n^0$, appear in the equations for the average cross section. The parameters for neutrons of angular momentum $\ell = 1$ were not known previously, but it is felt that the level spacing, D, and the radiation width, Γ_γ, may be about the same for $\ell = 0$ and $\ell = 1$.

The theoretical fit to the experimental points was obtained by varying $(\Gamma_\gamma/\bar{\Gamma}_n^0)_{\ell=1}$ as a first choice. The ratio, $(\Gamma_\gamma/\bar{D})_{\ell=1}$, was varied if a fit could not be obtained by variation of $(\Gamma_\gamma/\bar{\Gamma}_n^0)_{\ell=1}$. The parameters for neutrons with $\ell = 1$ are:

$$\left(\frac{\Gamma_\gamma}{D}\right)_{\ell=1} = \left(\frac{\Gamma_\gamma}{D}\right)_{\ell=0} \; ; \; \left(\frac{\Gamma_\gamma}{\Gamma_n^0}\right)_{\ell=1} = \frac{1}{4}\left(\frac{\Gamma_\gamma}{\Gamma_n^0}\right)_{\ell=0} \; ; \; \left(\frac{\bar{\Gamma}_n^0}{D}\right)_{\ell=1} = 2.0 \times 10^{-4}$$

In order to get this fit, we must assume an increase in the ratio $(\bar{\Gamma}_n^0/\bar{D})_{\ell=1}$ of 4 times the value given for the $\ell = 0$ ratio. The increase also seems to be predicted by the theory (F2) for nuclei of mass near 100.

Fig. 10 shows the calculated curve using equation 2.15, which gives the average capture cross section when we assume the distribution

function, $e^{-y}\sqrt{(y)}$, where $y = \Gamma_n^0/\bar{\Gamma}_n$. The parameters for the best fit are:

$\ell = 0$ $\quad \bar{D} = 32$ ev $\quad \bar{\Gamma}_n^0/\bar{D} = 0.625 \times 10^{-4}$

$\Gamma_\gamma = 0.13$ ev

$\bar{\Gamma}_n^0 = 2.0$ mv $\quad \Gamma_\gamma/_D = 4.1 \times 10^{-3}$

$\ell = 1$

$$\left(\frac{\Gamma_\gamma}{\bar{D}}\right)_{\ell=1} = \left(\frac{\Gamma_\gamma}{\bar{D}}\right)_{\ell=0} ; \quad \left(\frac{\Gamma_\gamma}{\bar{\Gamma}_n^0}\right)_{\ell=1} = \frac{1}{5}\left(\frac{\Gamma_\gamma}{\bar{\Gamma}_n^0}\right)_{\ell=0} ; \quad \left(\frac{\bar{\Gamma}_n^0}{\bar{D}}\right)_{\ell=1} = 3.1 \times 10^{-4}$$

In this case, it was found necessary to vary D within the limits of the Brookhaven value. Again, it was necessary to increase the ratio, $(\bar{\Gamma}_n^0/\bar{D})_{\ell=1}$ to obtain a fit. The increase is by a factor of 5 over the $\ell = 0$ ratio.

Using both distributions, good fits to the experimental points are obtained. Therefore, no conclusions can be drawn as to which distribution function is preferred. On the other hand, it can be stated that the p-wave contribution has a maximum in the region of 10 kev, which gives a flattening effect to the cross section in this region. Contributions to the cross section from higher angular momenta neutrons ($\ell \geq 2$) are assumed to come in at energies higher than the region considered here.

CAPTURE CROSS SECTION OF In^{115}

Normal Indium was used in the form of a foil 0.005 inches thick, 0.1 inch wide and 2.5 inches long. Neutron bombardment of this foil causes the following reaction to occur:

$$In^{115} + n^0 \longrightarrow In^{116} + \gamma$$

$$In^{116} \longrightarrow Sn^{116} + \beta^-$$

The half-life for the decay of the induced activity in In^{116} is 54 minutes. To approach saturation of the induced activity in this sample would

require a bombardment of approximately three hours per point. In order to reduce this time and still retain good statistics in the decays, the background of the beta counter was reduced. This was done as described in Chapter IV with the result that we had a beta background which was nearly constant at 5 c.p.m. The exposure time for each sample was one hour. Some decay curves are shown in Fig. 11. The solid line has the proper slope and was drawn as a best fit to the data.

In^{113} was also present in the sample, and the following reaction occurred:

$$In^{113} + n^{0} \longrightarrow In^{114} + \gamma$$

In^{114} is beta active and exists as an isomer with half-lives of 50 days and 72 seconds. The branching ratio for these two states is 30 to 1. Hence, very little of the In^{114} activity will be observed. This, coupled with the fact that In^{113} is only 4.2% abundant, makes the activity due to In^{114} negligibly small.

Eight experimental points were obtained in the region 5 kev to 250 kev. These points are shown in Fig. 12 and are again normalized to the Los Alamos points at the high energies. The resonance parameters are given by Harvey, et al (H5) for the region 1 ev to 150 ev. Again, these parameters were assumed to be the same for $\ell = 0$ neutrons in the kev region to obtain a best fit from equation 2.14.

The solid line in Fig. 12 is a sum of the contributions to the cross section due to neutrons of angular momentum $\ell = 0$ and $\ell = 1$. The distribution function used to obtain this curve was e^{-y} (calculated from equation 2.14). The parameters used to obtain this fit are:

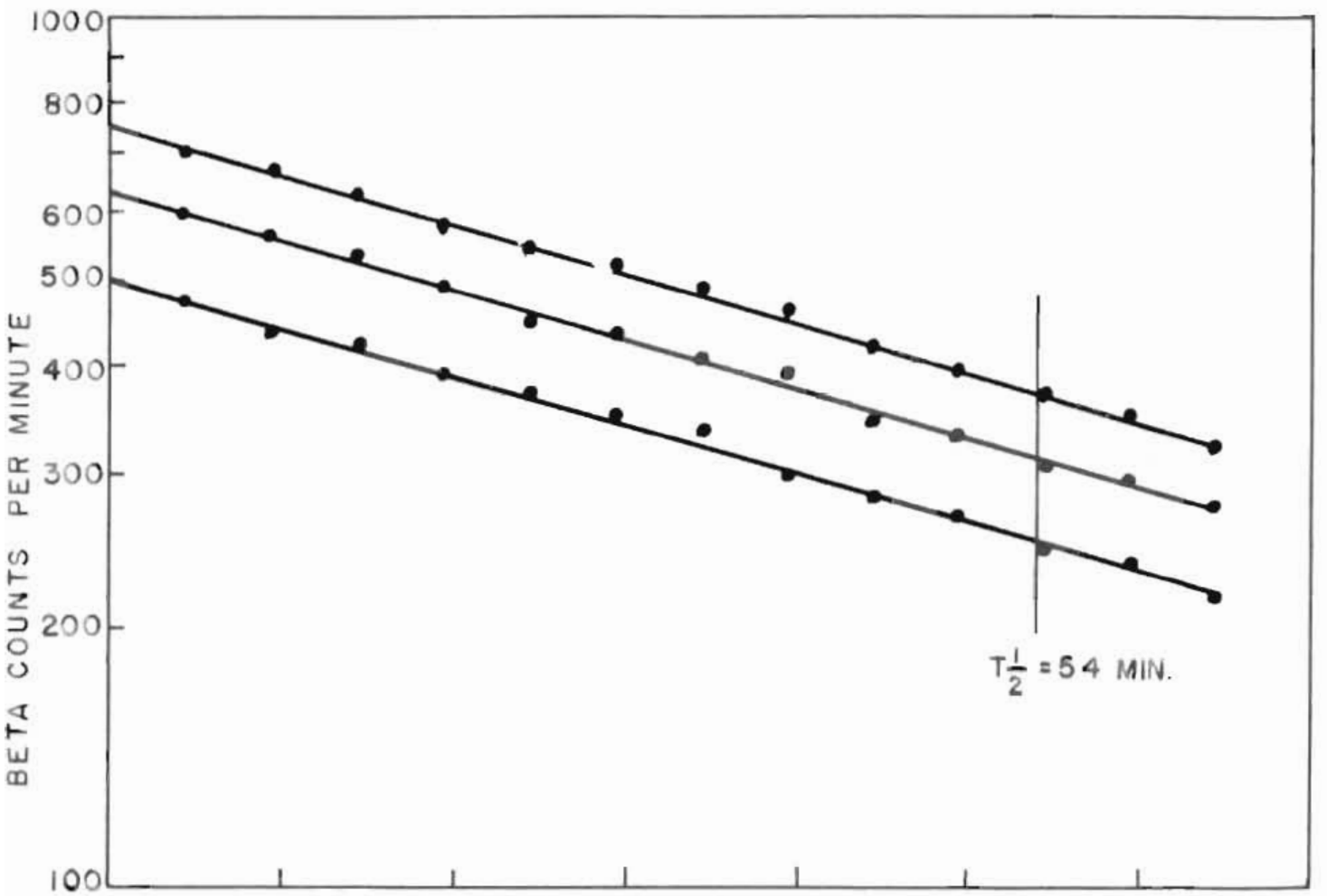

FIG. 11 TYPICAL DECAY CURVES OF In^{116}

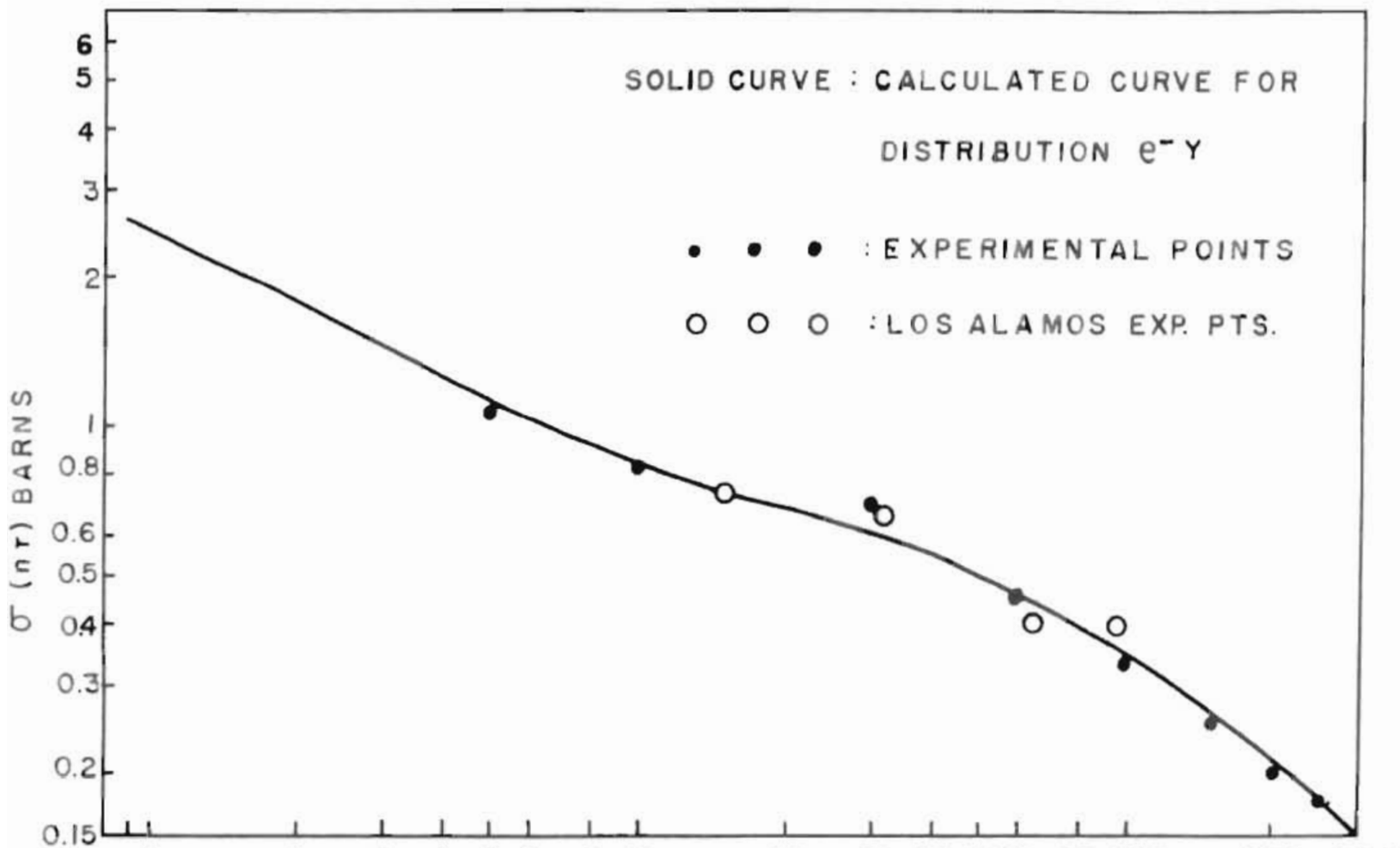

FIG. 12 NEUTRON CAPTURE CROSS SECTION OF In^{115}

$\ell = 0$ $\quad \bar{D} = 16$ ev

$\Gamma_\gamma = 77$ mv $\quad \bar{\Gamma}_n^0/\bar{D} = 0.27 \times 10^{-4}$

$\bar{\Gamma}_n^0 = 0.43$ mv $\quad \Gamma_\gamma/\bar{D} = 4.8 \times 10^{-3}$

$\ell = 1$

$$\left(\frac{\Gamma_\gamma}{D}\right)_{\ell=1} = \left(\frac{\Gamma_\gamma}{D}\right)_{\ell=0}, \left(\frac{\Gamma_\gamma}{\Gamma_n^0}\right)_{\ell=1} = \frac{1}{4}\left(\frac{\Gamma_\gamma}{\Gamma_n^0}\right)_{\ell=0}; \quad \left(\frac{\bar{\Gamma}_n^0}{D}\right)_{\ell=1} = 1.08 \times 10^{-4}$$

Harvey (H5) gives a value of 14 ± 2 ev for $\bar{D}$. It was found necessary to give $\bar{D}$ a value of 16 ev to obtain the above fit.

Fig. 13 gives the best fit of the theoretical capture cross section using equation 2.15. This equation gives the average capture cross section when the reduced neutron width is weighted with the distribution function $e^{-y/2}/(y)^{\frac{1}{2}}$. The parameters used in this case are:

$\ell = 0$

$\bar{D} = 14$ ev

$\Gamma_\gamma = 77$ mv $\quad \bar{\Gamma}_n^0/\bar{D} = 0.31 \times 10^{-4}$

$\bar{\Gamma}_n^0 = 0.43$ mv $\quad \Gamma_\gamma/\bar{D} = 5.5 \times 10^{-3}$

$\ell = 1$

$$\left(\frac{\Gamma_\gamma}{D}\right)_{\ell=1} = \left(\frac{\Gamma_\gamma}{D}\right)_{\ell=0}; \quad \left(\frac{\Gamma_\gamma}{\Gamma_n^0}\right)_{\ell=1} = \frac{1}{4}\left(\frac{\Gamma_\gamma}{\Gamma_n^0}\right)_{\ell=0}; \quad \left(\frac{\bar{\Gamma}_n^0}{\bar{D}}\right)_{\ell=1} = 1.24 \times 10^{-4}$$

As in the case of silver, both distributions give reasonably good fits to the experimental points. Therefore, at this point we cannot prefer one distribution over the other. In both cases, the p-wave contribution has a maximum in the region of 20 kev, which causes an almost constant capture cross section in this region. For the $\ell = 1$ neutrons, we are forced to increase the ratio, $\left(\bar{\Gamma}_n^0/\bar{D}\right)_{\ell=1}$, over the $\ell = 0$ ratio,

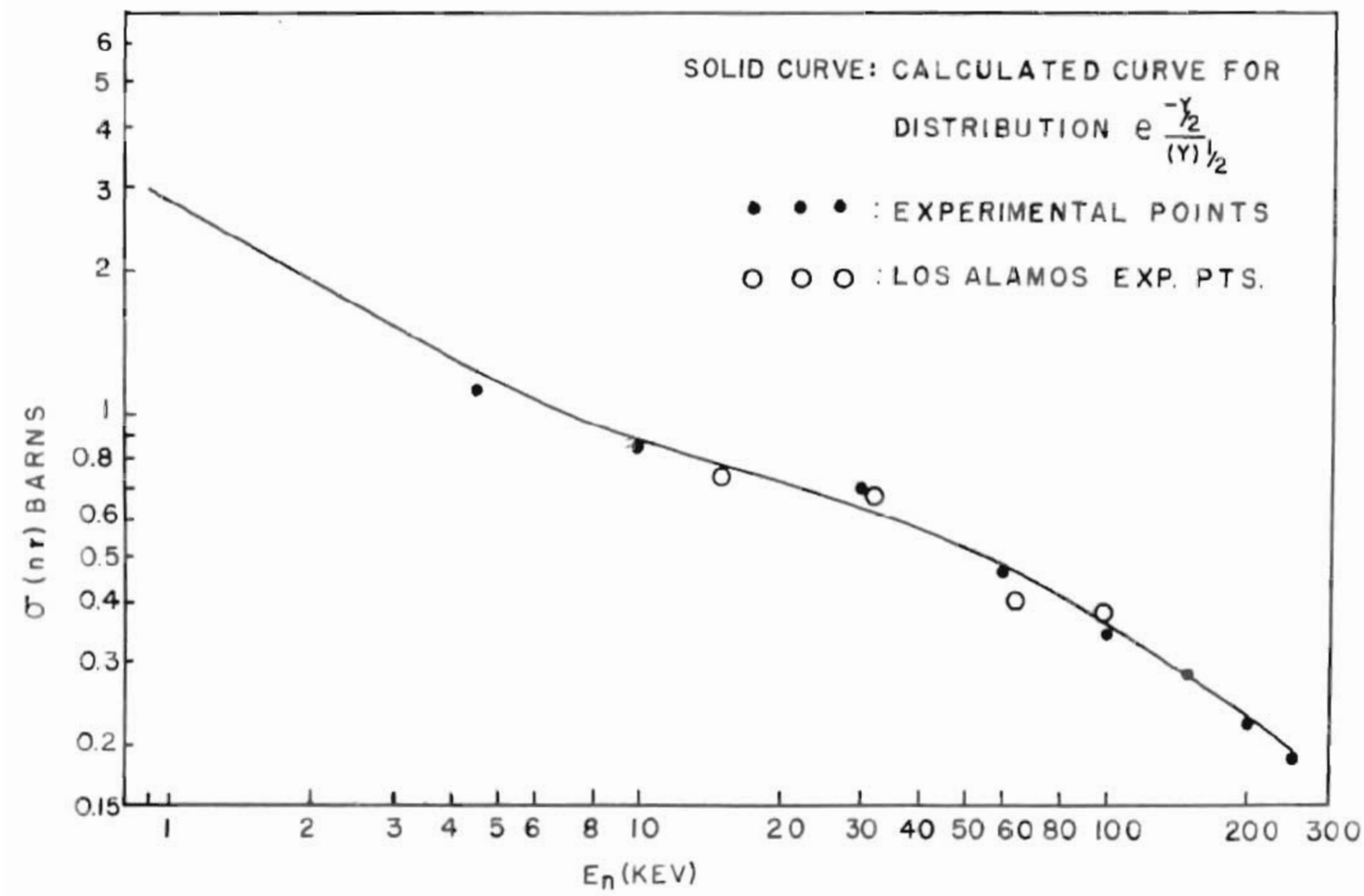

FIG. 13 NEUTRON CAPTURE CROSS SECTION OF In^{115}

but to a lesser degree than in the case of silver. The theory (F2) predicts that for ℓ = 1 neutrons, this ratio decreases for elements progressively further away from mass number 100.

From this work, we can neither say where nor to what degree the higher angular momenta terms ($\ell \geq 2$) contribute to the capture cross section. We do believe, however, that these contributions come at energies above 200 kev, but to a much lesser degree.than the ℓ = 1 term.

Up to this point, nothing has been said about the isomer of In^{116} which has a half-life of 13 seconds. The two isomers, 54 minutes and 13 seconds, have a branching ratio of 145 to 52. The resonance parameters given by Brookhaven are given for both isomers, but these parameters have an error of approximately 25%. If this error did not exist, the radiation width, Γ_γ, would have to be reduced by 25%, i.e. to 77 x 145/197 = 57 mv. We used a value of Γ_γ = 77 mv for both distributions. This value lies within the experimental error of the value given by Brookhaven for the 54 min. isomer.

CAPTURE CROSS SECTION OF U^{238}

Since U^{238} eventually decays into Pb, there are a large number of daughter products present in any sample of this element; many of these are beta active. In our samples, this beta activity was approximately 100,000 c.p.m. and would tend to mask any activity which might have been induced in a sample by neutron bombardment. Therefore, to obtain the capture cross section by the method proposed in this paper, we had to separate the U sample in such a way that the natural beta activity was

several times below the strength of the induced activity.

In our first attempts, we activated uranium foil and tried to separate the uranium from its daughter products. This separation required one and one-half hours, in which time the induced activity of U^{239} (23 minute half-life) decayed by a factor of 8. The natural activity of the sample was reduced to 3,000 c.p.m., which was three to four times the counting rate expected from the induced activity. We abandoned this method because the separation required too long a time and was not completely successful.

Success was finally achieved by performing the separation before the activation. This separation was performed in a manner similar to that described by Anderson (A3). Four grams of uranyl nitrate $UO_2(NO_3)_2 \cdot 6H_2O$ was dissolved in 100 c.c. of ether and the mixture poured into a separatory funnel. The water component was then drained off; this water contained the dissolved daughter products. We then added 6 drops of water to the ether solution and thoroughly mixed. The water was again drained off, and the process was repeated four times. Because water is about 5% soluble in ether, some of the daughter products were still present in the ether solution. In order to remove these daughter products, a deliquescent substance ($MgSO_4$) was added. $MgSO_4$ is not soluble in ether and absorbs the water as it filters through the ether solution. The ether solution, free of daughter products, was then poured into a large watch glass and heated to evaporate the ether as quickly as possible. The end product was pure uranyl nitrate. By heating this compound to a red heat, it decomposes to U_3O_8.

U_3O_8 was then in the form of a powder and had to be pressed into a ring in order to be used as a sample. Oxygen, which was present in the sample, has a total cross section of 3.5 barns that is constant up to an energy of 300 kev. O^{16} is 99.76 per cent abundant; O^{17} and O^{18} are stable. Consequently, we did not expect any beta activity (due to neutron capture) from this element.

The U_3O_8 ring had a width of 1/8", inside radius of 0.4" and a thickness of 0.1". The mass in each sample was 1.6$\pm$.1 grams. The total time to make a ring was one hour, and the natural background of a sample an hour after the separation was in the neighborhood of 200 c.p.m. The build-up of activity due to daughter products was followed for five days and found to be constant within statistics. This build-up of activity varied slightly for each ring, but was generally in the neighborhood of 120 c.p.m. per hour. Because of this build-up of natural background, each sample had to be made immediately before each exposure.

The build-up curve of each sample had to be known. This was found by counting the sample before each exposure and for several days afterwards. Once this curve was known, the proper number of counts could be subtracted from the counting rate during the decay. Since the natural activity increased at a constant rate, recording of the time was a very important component in the activation of U^{238}.

Because of the build-up of activity in the sample, the exposure time was set at 30 minutes. With this exposure time, induced activities of 500 to 1200 c.p.m. were obtained. Fig. 14 gives a typical decay curve,

which has been corrected for beta counter background and for background due to decay of daughter products. Fig. 15 gives the build-up curve for the sample whose decay is shown in Fig. 14. U^{238} decays by alpha emission to Th^{234} which has a half-life of 24 days. Th^{234} then beta decays and, therefore, is the primary constituent of the build-up curve.

When U^{238} captures a neutron, the following reaction occurs:

$$U^{238} + n \rightarrow U^{239} + \gamma$$

$$U^{239} \rightarrow Np^{239} + \beta^-$$

Although Np^{239} is unstable and beta decays, very few beta counts were due to this element in the initial period since it has a half-life of 2.33 days.

For ℓ = 0 neutrons, the resonance parameters (H4) for U^{238} are:

$\bar{D}$ = 19 ev

Γ_γ = 23 mv $\qquad \bar{\Gamma}_n^0/\bar{D} = 1.4 \times 10^{-4}$

$\bar{\Gamma}_n$ = 2.8 mv

These parameters are within the limits of error for the same as those given by Harvey, et al (H5).

Sixteen experimental points were obtained in the region 3 kev to 220 kev. These points are shown in Fig. 16 and Fig. 17 normalized to the Los Alamos (A1) points for the capture cross section of U^{238}.

The solid line in Fig. 16 shows the best fit using equation 2.14 and the distribution $\bar{e}^{\gamma}$ in calculating the capture cross section. The parameters used are:

$\ell = 0$ $\qquad \bar{D}$ = 19 ev

Γ_γ = 23 mv $\qquad \bar{\Gamma}_n^0/\bar{D} = 1.4 \times 10^{-4}$

$\bar{\Gamma}_n^0$ = 2.8 mv $\qquad \Gamma_\gamma/\bar{D} = 1.2 \times 10^{-3}$

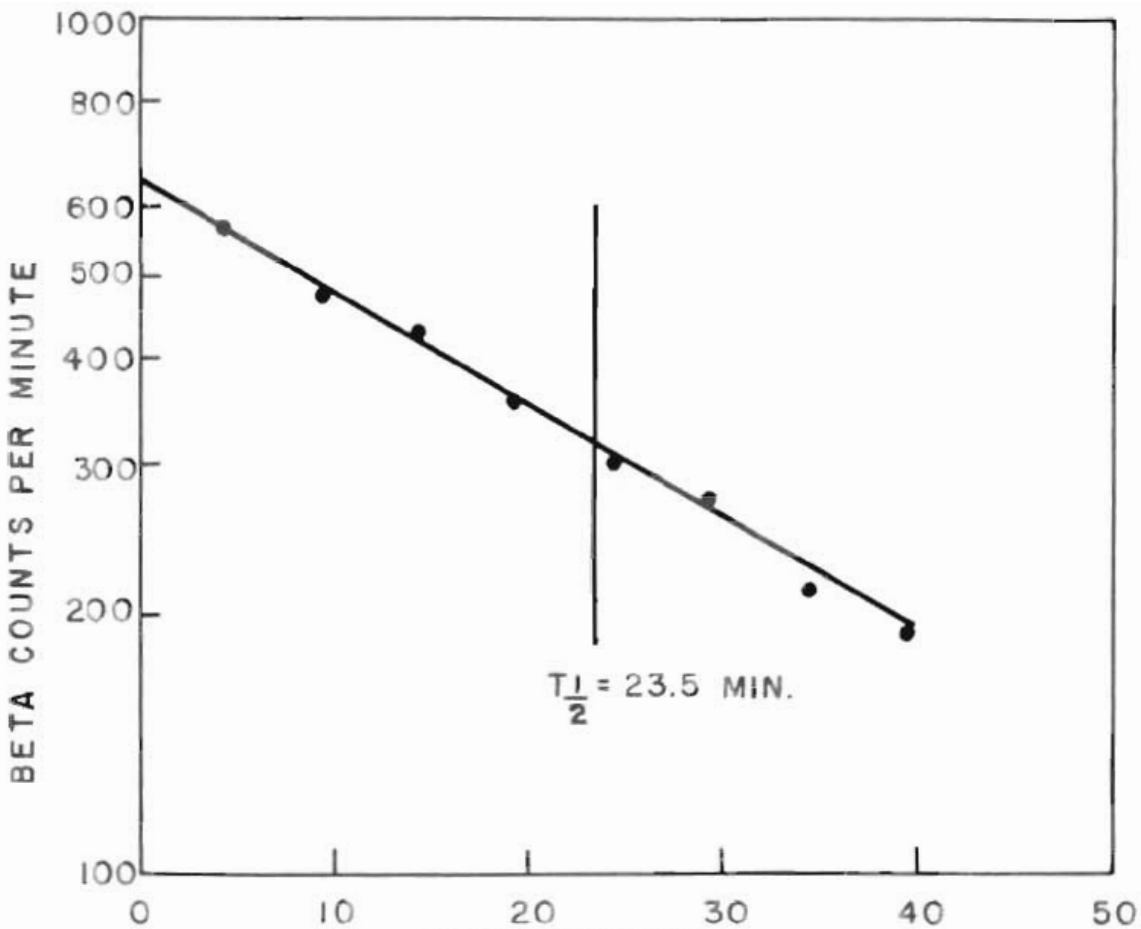

FIG. 14 TYPICAL DECAY CURVE OF U^{239}

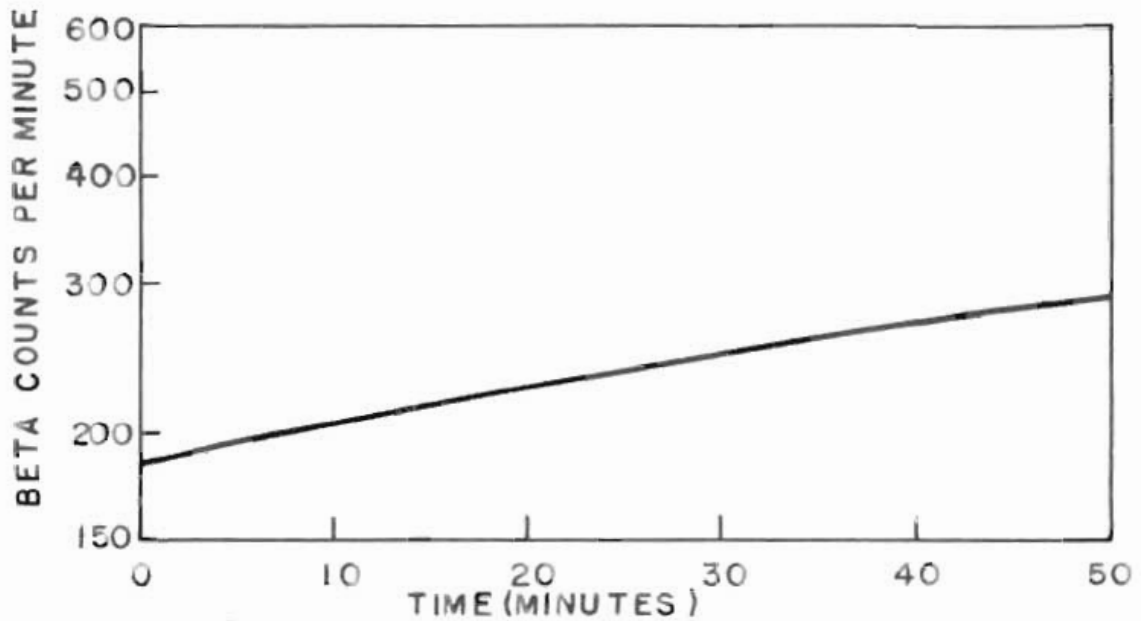

FIG. 15 ACTIVITY BUILD-UP IN URANIUM SAMPLE DUE TO Th^{234}

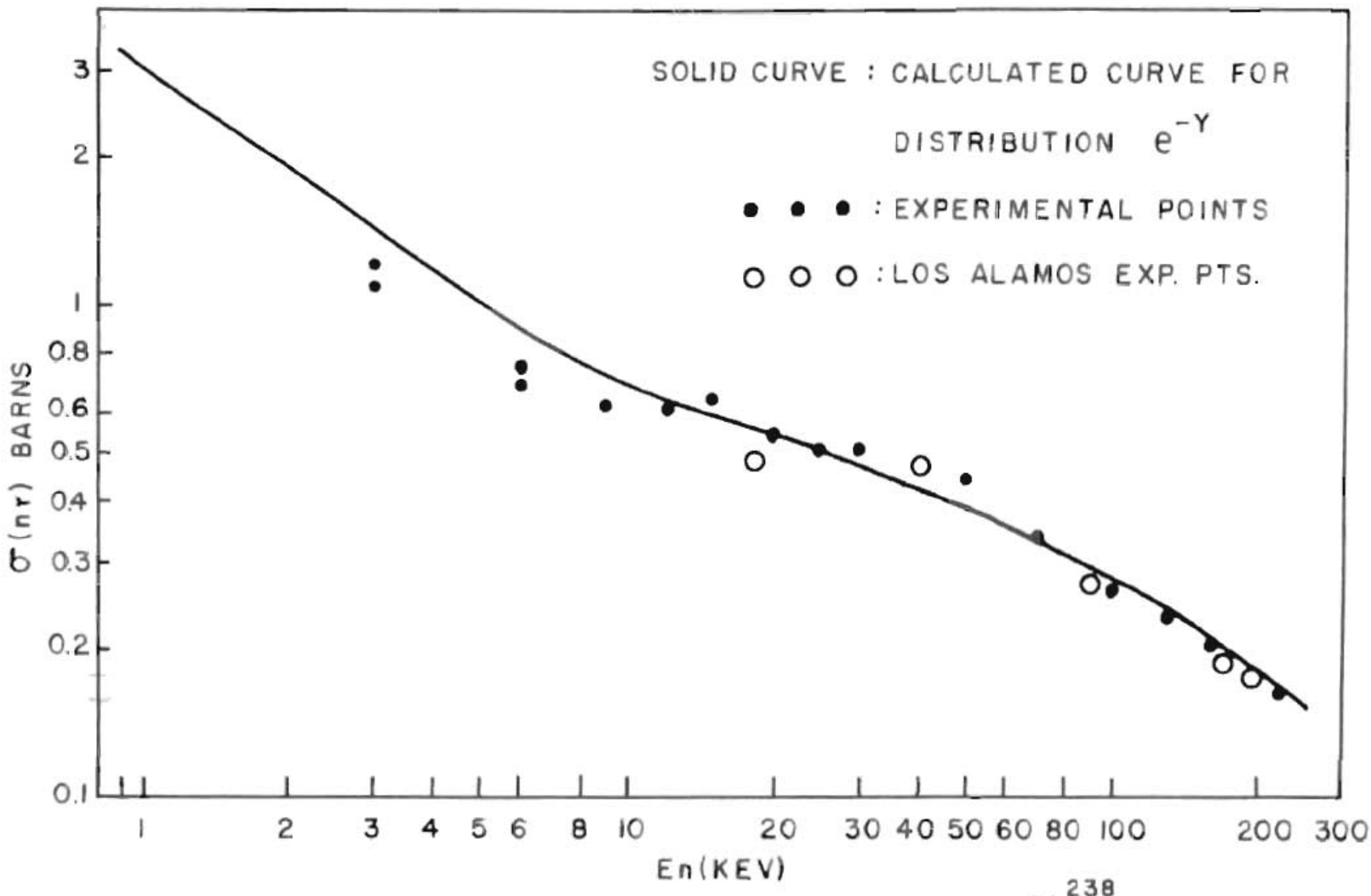

FIG. 16 NEUTRON CAPTURE CROSS SECTION OF U^{238}

$\ell = 1$

$$\left(\frac{\Gamma_\nu}{D}\right)_{\ell=1} = 2\left(\frac{\Gamma_\nu}{D}\right)_{\ell=0} \; ; \; \left(\frac{\Gamma_\nu}{\Gamma_n^0}\right)_{\ell=1} = 4\left(\frac{\Gamma_\nu}{\Gamma_n^0}\right)_{\ell=0} \; ; \; \left(\frac{\overline{\Gamma_n^0}}{D}\right)_{\ell=1} = 0.7 \times 10^{-4}$$

The solid line in Fig. 17 gives the theoretical fit using equation 3.15 and the distribution $e^{-y/2}/y^{1/2}$ in calculating the capture cross section. The resonance parameters are:

$\ell = 0$ $\quad \overline{D} = 19$ ev

$\Gamma_\nu = 23$ mv $\quad \overline{\Gamma_n^0}/\overline{D} = 1.4 \times 10^{-4}$

$\overline{\Gamma_n^0} = 3.8$ mv $\quad \Gamma_\nu/\overline{D} = 1.2 \times \times 10^{-3}$

$\ell = 1$

$$\left(\frac{\Gamma_\nu}{D}\right)_{\ell=1} = 3\left(\frac{\Gamma_\nu}{D}\right)_{\ell=0} \; ; \; \left(\frac{\Gamma_\nu}{\Gamma_n^0}\right)_{\ell=1} = 6\left(\frac{\Gamma_\nu}{\Gamma_n^0}\right)_{\ell=0} \; ; \; \frac{\overline{\Gamma_n^0}}{D} = 0.7 \times 10^{-4}$$

It is interesting to note that both distributions cause the ratio, $\overline{\Gamma}_n^0/\overline{D}$, for $\ell = 1$ to decrease with respect to the ratio for $\ell = 0$ neutrons. Both distributions give exactly the same ratio for $\ell = 1$ neutrons.

The distribution $e^{-y/2}/y^{1/2}$ seems to give a better fit at low energies making this distribution the preferred one.

Work now in progress seems to indicate that the contribution to the capture cross section of U^{238} due to $\ell = 2$ neutrons is negligible at all neutron energies. We believe that this is due to inelastic scattering which becomes important in the region (100 kev to 300 kev) where we would normally expect $\ell = 2$ neutrons to become important.

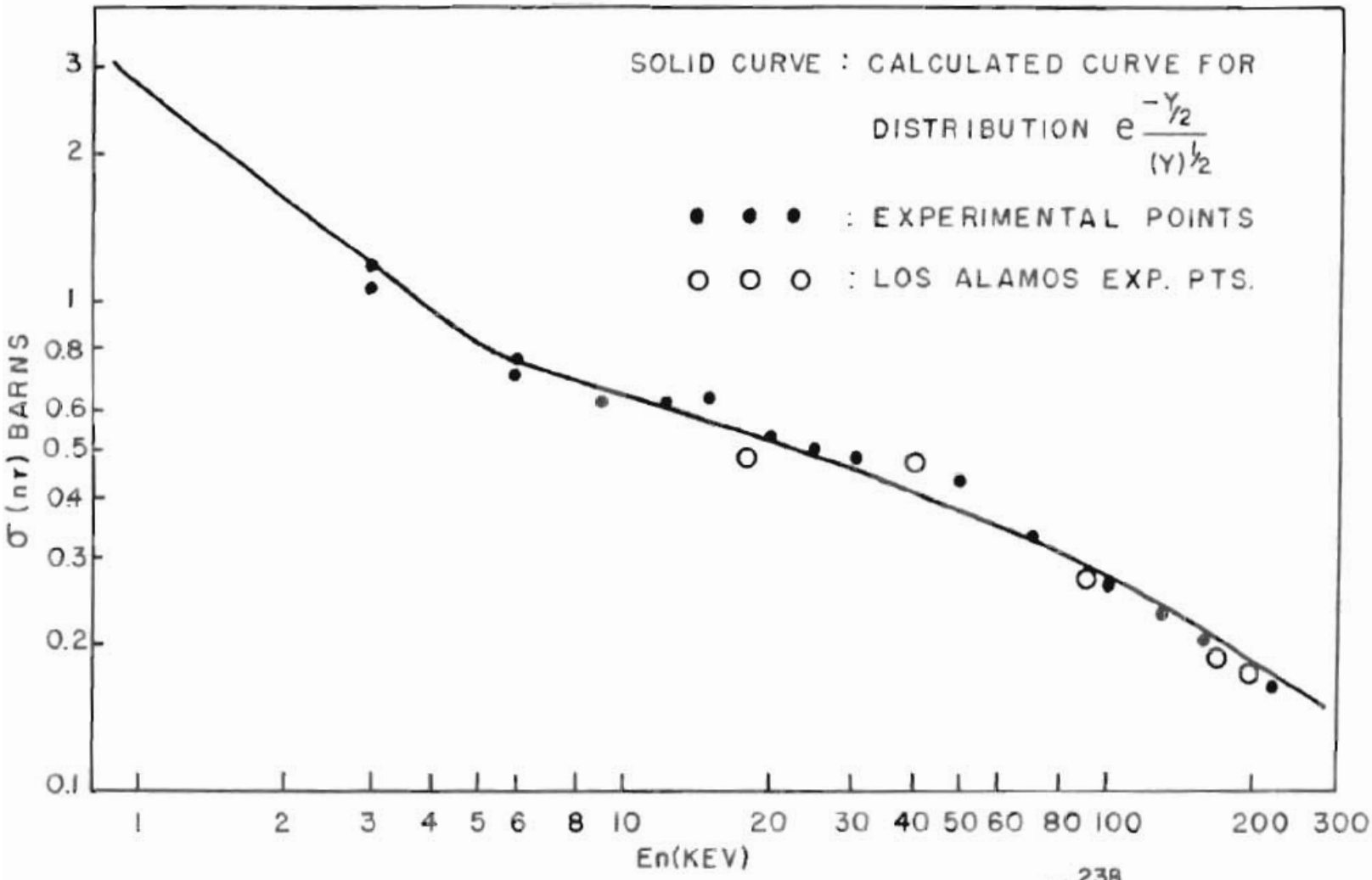

FIG. 17 NEUTRON CAPTURE CROSS SECTION OF U^{238}

In order to summarize all the parameters of Ag^{107}, In^{115} and U^{238}, Table I has been tabulated. This table shows the parameters which give a satisfactory fit to our experimental points. T-P refers to the Thomas-Portor distribution $e^{-y/2}/y^{1/2}$ and Exp. refers to the distribution e^{-y}.

The uniform distribution was also used in the analysis of the cross section curves. This distribution gave poor results in all cases.

TABLE I

SUMMARY OF THE PARAMETERS

	1/2 Life	$\bar{\Gamma}_{n}/\bar{D} \times 10^{3}$ $\ell = 0$	$\bar{\Gamma}_{\gamma}/\bar{D} \times 10^{3}$ $\ell = 0$	$\bar{\Gamma}_{n^0}/\bar{D} \times 10^{4}$ $\ell = 0$	Distribution Function	$\bar{\Gamma}_{\gamma}/\bar{D} \times 10^{3}$ $\ell = 1$	$\bar{\Gamma}_{n}/\bar{D} \times 10^{4}$ $\ell = 1$
U^{238}	23.5 min	1.6 - 1.3*	1.2	1.4	T - P	3.6	0.7
U^{238}	23.5 min		1.2	1.4	Exp	2.4	0.7
U^{238}	23.5 min		1.2	1.4	Uniform	-	-
In^{115}	54 min	4.7 - 3.5*	5.5	0.31	T - P	5.5	1.24
In^{115}	54 min		4.8	0.27	Exp	4.8	1.08
In^{115}	54 min		4.0	0.31	Uniform	-	-
Ag^{107}	2.3 min	4.3 - 2.6*	4.1	0.625	T - P	4.1	3.1
Ag^{107}	2.3 min		3.25	0.50	Exp	3.25	2.0
Ag^{107}	2.3 min		2.9	0.50	Uniform	-	-

*Brookhaven values.

APPENDIX

Solution of the integral $\int_0^\infty \frac{v^2 e^{-v^2}}{v^2+b}\,dv$

The above integral can be separated into two parts.

$$\int_0^\infty \frac{v^2 e^{-v^2}}{v^2+b}\,dv = \int_0^\infty e^{-v^2}\,dv - b\int_0^\infty \frac{e^{-v^2}}{v^2+b}\,dv$$

The first integral can be integrated directly giving:

$$\int_0^\infty e^{-v^2}\,dv = \frac{\sqrt{\pi}}{2}$$

The second integral we shall call I.

Therefore, $I = \int_0^\infty \frac{e^{-v^2}}{v^2+b}\,dv = e^b \int_0^\infty \frac{e^{-(v^2+b)}}{v^2+b}\,dv$

We now write thisintegral in a slightly new form.

$$I(\lambda) = e^b \int_0^\infty \frac{e^{-\lambda(v^2+b)}}{v^2+b}\,dv \qquad \left[I = I(\lambda=1)\right]$$

We will now assume a new integral which can be integrated and which will be related to I(λ) by a series of operations.

$$\phi(\lambda) = e^b \int_0^\infty e^{-\lambda(v^2+b)}\,dv = e^{b(1-\lambda)} \int_0^\infty e^{-\lambda v^2}\,dv = e^{b(1-\lambda)} \frac{1}{2}\sqrt{\frac{\pi}{\lambda}}$$

Now, instead of solving the new integral, we will perform an integration with respect to λ'.

$$\int_0^\lambda \phi(\lambda')\,d\lambda' = e^b \int_0^\lambda \int_0^\infty e^{-\lambda'(v^2+b)}\,dv\,d\lambda'$$

We then perform the integration over λ'.

$$\int_0^\lambda \phi(\lambda')\,d\lambda' = e^b \int_0^\infty \frac{e^{-\lambda'(v^2+b)}}{-(v^2+b)}\,dv \Big|_0^\lambda$$

$$= -e^{+b} \int_0^{\infty} \frac{e^{-\lambda(v^2+b)}}{v^2+b}\, dv + e^{b} \int_0^{\infty} \frac{dv}{v^2+b}$$

The first integral is just $I(\lambda)$ and the second is solvable.

$$\int_0^{\lambda} \Phi(\lambda')\, d\lambda' = -I(\lambda) + e^{b} \frac{\pi}{2\sqrt{b}}$$

We already know that $\Phi(\lambda) = e^{b(1-\lambda)} \frac{1}{2}\sqrt{\frac{\pi}{\lambda}}$

Therefore: $-I(\lambda) + e^{b} \frac{\pi}{2\sqrt{b}} = \int_0^{\lambda} e^{b(1-\lambda')} \frac{1}{2}\sqrt{\frac{\pi}{\lambda'}}\, d\lambda' = \frac{\sqrt{\pi}}{2} e^{b} \int_0^{\lambda} \frac{e^{-b\lambda'}}{\sqrt{\lambda'}}\, d\lambda'$

In order to simplify the last integral, we make the following substitution;

let $b\lambda' = t^2$ $\qquad d\lambda' = 2t\,dt/b$

$\lambda' = 0 \qquad t = 0$

$\lambda' = \lambda \qquad t = \sqrt{b\lambda}$

Hence: $I(\lambda) = e^{b} \frac{\pi}{2\sqrt{b}} - e^{b} \frac{\sqrt{\pi}}{\sqrt{b}} \int_0^{\sqrt{b\lambda}} e^{-t^2} dt$

We will now solve the integral when $\lambda = 1$ which gives;

$$I = e^{b} \frac{\pi}{2\sqrt{b}} - e^{b} \frac{\sqrt{\pi}}{\sqrt{b}} \int_0^{\sqrt{b}} e^{-t^2} dt$$

The integral $\int_0^{\sqrt{b}} e^{-t^2} dt$ is the "error function" which is a tabulated integral.

The original integral can now be written in terms of the error function.

$$\int_0^{\infty} \frac{v^2 e^{-v^2}}{v^2+b}\, dv = \frac{\sqrt{\pi}}{2} - b\left(e^{b} \frac{\pi}{2\sqrt{b}} - e^{b} \frac{\sqrt{\pi}}{\sqrt{b}} \int_0^{\sqrt{b}} e^{-t^2} dt \right)$$

Simplifying, we have

$$\int_0^{\infty} \frac{v^2 e^{-v^2}}{v^2+b}\, dv = \frac{\sqrt{\pi}}{2} - e^{b} \frac{\sqrt{b\pi}}{2} \left(\sqrt{\pi} - 2 \int_0^{\sqrt{b}} e^{-t^2} dt \right)$$

BIBLIOGRAPHY

(A1) AECU 2040, Neutron Cross Sections, Technical Information Service, Oak Ridge, Tenn.

(A2) Albert, R. D. and E. R. Gaerttner, "Measurement of Neutron Capture Resonances Using an (n,γ) Scintillation Detector," Physical Review 91, 451, (1953).

(A3) Anderson, H. L., "Resonance Capture of Neutrons by Uranium," Physical Review 80, 499, (1950).

(B1) Bethe, H. A., "Nuclear Physics," Reviews of Modern Physics 9, 140, (1937).

(B2) Bethe, H. A. and G. Placzek, Resonance Effects in Nuclear Processes," Physical Review 51, 450, (1937).

(B3) Blatt, J. M. and V. F. Weisskopf, Theoretical Nuclear Physics. New York: John Wiley & Sons, Inc., (1947).

(B4) Breit, G. and E. P. Wigner, "Capture of Slow Neutrons," Physical Review 49, 519, (1936).

(C1) Capp, P., "Capture Cross Section of Thallium," Unpublished M.S. Thesis, Duke University, (1955).

(C2) Carter, R. S., J. A. Harvey, D. S. Hughes and V. E. Pilcher, "Ratio of Γ_n/D for Slow Neutron Resonances," Physical Review 96, 113, (1954).

(F1) Feshbach, H., D.C. Peaslee and V. F. Weisskopf, "On the Scattering and Absorption of Particles By Atomic Nuclei," Physical Review 71, 145, (1947).

(F2) Feshbach, H., C. E. Porter and V. F. Weisskopf, "Model for Nuclear Reactions with Neutrons," Physical Review 96, 448, (1954).

(F3) Fowler, W. A., G. R. Burbidge and E. M. Burbidge, "Nuclear Reactions and Element Synthesis in the Surfaces of Stars," The Astrophysical Journal, Supplement No. 17 2, 167, (1955).

(F4) Fowler, W. A., G. R. Burbidge and E. M. Burbidge, "Stellar Evolution and the Synthesis of the Elements," The Astrophysical Journal 122, 271, (1955).

(G1) Gamow, G., "On Relativistic Cosmogony," Reviews of Modern Physics 21, 367, (1949).

(H1) Hanson, H. O. and J. L. McKibben, "A Neutron Detector Having Uniform

Sensitivity from 10 Kev to 3 Mev," Physical Review 72, 673, (1947).

(H2) Hanson, A.O., R. F. Taschek and J. H. Williams, "Monoergic Neutrons from Charged Particle Reactions," Reviews of Modern Physics 21, 635, (1949).

(H3) Harris, S. P., C. O. Muehlhause and G. E. Thomas, "Low Energy Neutron Resonance Scattering and Absorption," Physical Review 79, 11, (1950).

(H4) Harvey, J. A., Private Communication, Brookhaven National Laboratory, (1955).

(H5) Harvey, J. A., D. J. Hughes, R. S. Carter, and V. E. Pilcher, "Spacing and Neutron Widths of Nuclear Energy Levels," Physical Review 99, 10, (1955).

(H6) Harvey, J. A., C. E. Porter and D. J. Hughes, "Variation of the Ratio with Atomic Weight," Physical Review 98, 645, (1954).

(H7) Hibdon, C. T. and C. O. Muehlhause, "Neutron Cross Sections at 115 ev and 300 ev," Physical Review 76, 100, (1949).

(H8) Hibdon, C. T. and C. O. Muehlhause, ANL-4552, 6.

(H9) Hughes, D. J., "Radiation Widths of Nuclear Energy Levels," Nature 173, 942, (1954).

(H10) Hughes, D. J., R. C. Garth and J. S. Levin, "Fast Neutron Cross Sections and Nuclear Level Density," Physical Review 91, 1423, (1953).

(H11) Hughes, D. J. and J. A. Harvey, "Size Distribution of Neutron Widths," Physical Review 99, 1032, (1955).

(H12) Hughes, D. J., W. D. B. Spatz and N. Goldstein, "Capture Cross Sections for Fast Neutrons," Physical Review 75, 1781, (1949).

(J1) Johannsson, Sven A. E., "Decay of UX, UX_2 and UZ," Physical Review 96, 1075, (1954).

(J2) Johnson, W. G., "A Cloud Chamber Study of the Decoherence Curve for Small Counter Separation," Unpublished Thesis, University of North Carolina, 1955.

(L1) Landon, H. H. and V. L. Sailor, "Radiation Width Variations in the Slow Neutron Resonances of Europium and Indium," Physical Review 98, 1267, (1955).

(M1) Meservey, E., "Neutron Capture Cross Sections by Capture-Gamma Counting," Physical Review 98, 1006, (1954).

(M2) Montgomery, D. J. X., Cosmic Ray Physics, Princeton: Princeton University Press, 1949.

(M3) Muehlhause, C. O., "Neutron Capture Gamma-Ray Multiplicity," Physical Review 79, 277, (1950).

(R1) Rohrer, R. H., "Neutron Resonances in Selected Nuclides," Unpublished Thesis, Duke University, 1954.

(R2) Rohrer, R. H., Private Communication, Duke University, 1955.

(R3) Rose, B., "A Determination of the Cross Section for the Reaction $U^{238}(n,\gamma)U^{239}$ as a Function of Neutron Energy in the Range 30-900 Kev," A. E. R. E. Harwell NP/R 1743.

(R4) Rossi, B., "Interpretation of Cosmic-Ray Phenomena," Reviews of Modern Physics, 20, 537, (1948).

(S1) Sailor, V. L. and L. B. Borst, "Slow Neutron Resonances in In^{113} and In^{115}," Physical Review 87, 161, (1952).

(S2) Seidl, F. G. P., D. J. Hughes, H. Palevsky, J. S. Levin, W. Y. Kato and N. G. Sjostrand, " 'Fast Chopper' Time-of-Flight Measurement of Neutron Resonances," Physical Review 98, 476, (1954).

(S3) Soren, L., N. N. Friedlander and S. H. Turkel, "Thermal Neutron Activation Cross Sections," Physical Review 72, 888, (1947).

(T1) Tables of Sine, Cosine and Exponential Integrals, Vol. 2, Federal Works Agency, New York, 1940.

(T2) Tables of the Error Function and Its Derivative, National Bureau of Standards, Applied Mathematics Series 41, 1954.

(T3) Thomas, R. G., "Fluctuations of Nuclear Reaction Widths," Private Communication, Los Alamos Scientific Laboratory, Los Alamos, New Mexico.

(T4) Thomas, R. G., "On the Determination of Reduced Widths from the One-Level Dispersion Formula," Physical Review 81, 148, (1951).

(W1) Weisskopf, V. F., "Compound Nucleus and Nuclear Resonances," Helvetica Physica Acta 23, 185, (1950).

(W2) Wigner, E. P., "Nuclear Reactions and Level Widths," American Journal of Physics 17, 99, (1949).

(W3) Williamson, R. H., Private Communication, Duke University, 1955.

(W4) Wollan, E. O. and C. G. Shull, "Neutron Diffraction and Associated Studies," Nucleonics 3, 8, (1948).